ATOMIC OXYGEN EFFECTS ON PARTICULATE CONTAMINATION AND SHORT BEAM STRENGTH OF CARBON COMPOSITES

A Thesis

presented to

the Faculty of California Polytechnic State University

San Luis Obispo

In Partial Fulfillment

of the Requirements for the Degree

in Aerospace Engineering

by

Marlee Litzinger

June 2019

COMMITTEE MEMBERSHIP

TITLE:	Atomic Oxygen Effects on Particulate Contamination and Short Beam Strength of Carbon Composites
AUTHOR:	Marlee Litzinger
DATE SUBMITTED:	June 2019
COMMITTEE CHAIR:	Kira Abercromby, Ph.D. Associate Professor Aerospace Engineering Department
COMMITTEE MEMBER:	Amelia Greig, Ph.D. Associate Professor Aerospace Engineering Department
COMMITTEE MEMBER:	Kaveh Kabir, Ph.D. Lecturer Aerospace Engineering Department
COMMITTEE MEMBER:	Carlos Soares Contamination Control Engineer NASA Jet Propulsion Laboratory

ABSTRACT

Atomic Oxygen Effects on Particulate Contamination and Short Beam Strength of Carbon Composites

Marlee Litzinger

In order to design a successful space system, the unique challenges of the space environment it will operate in must be considered during the design process. Atomic oxygen (AO) is a detrimental environmental effect found in Low Earth Orbit (LEO) that affects spacecraft surfaces by oxidizing and eroding material over time, particularly polymers. Carbon fiber/epoxy composites are a commonly used spacecraft material affected by AO exposure. Carbon composites are used as a structural material, such as on solar panels; their large surface area therefore is a potential contamination source to sensitive components. The Space Environments and Testing Lab at California Polytechnic State University, San Luis Obispo (Cal Poly SLO) includes an apparatus that can simulate AO in the LEO environment. This apparatus was used to expose carbon composite samples to AO before being tested for short beam strength to measure the effect on material properties. Results showed no significant difference in short beam strength for a 24-hour AO exposure compared to unexposed samples, but a 4% decrease for samples with a 48-hour exposure. Previous work at Cal Poly SLO found that AO-exposed composite generated particulate contaminants. Tape lift tests and mass measurements of samples were conducted before and after AO exposure to characterize the particulate contamination generated and percent mass loss. It was found that AO exposure increased the percent mass loss by 1.5% for 24-hour exposure and 3% for 48-hour exposure. The tape lift percent area coverage increased by 2.5% near sample ends and 0.35% in the middle after AO exposure.

ACKNOWLEDGMENTS

I would like to thank Dr. Abercromby, for advising this thesis and supporting me throughout this journey; Dr. Greig, for serving on my committee and as Graduate Coordinator; Dr. Kabir, for serving on my committee and his support during sample preparation and structural testing; Carlos Soares, for serving on my committee and helping develop the contamination aspects of this thesis; Eric Beaton of the MATE department, for teaching me about microscopy for the contamination analysis; Daniel Fugett, for being a willing sounding board every step of the way; my friends, for their love, support, willing extra hands, and ability to sit with me in labs; and my family, for encouraging and supporting me every step of the way. I would not have been able to accomplish this without you.

TABLE OF CONTENTS

LIST OF TABLES

LIST OF FIGURES

Chapter 1

INTRODUCTION

This chapter will explore the importance of designing specifically for the space environment. The implications of the components of the space environment will be briefly discussed, with further information given in chapter 2 as it pertains specifically to this thesis topic. This chapter will end with the motivation for the completion of this thesis project.

1.1 Engineering for the Space Environment

When designing vehicles for the space environment, several categories of environmental conditions must be considered: the neutral environment, micrometeorites and orbital debris (MMOD), radiation, and plasma. These components can affect the performance of a spacecraft from incremental decreases to catastrophic failure. As shown in Table 1.1, the spacecraft design and environment are the largest source of spacecraft failure over time [1]. Without adequately addressing the challenges of the space environment, the spacecraft's ability to complete its mission is at risk.

Table 1.1: Trends in Spacecraft Failures [1]

Year	Design and Environment	Parts and Quality	Operational and Others	Unknown
Pre-1977	42	26	12	20
1977-1983	57	20	10	13
Most recent	36	11	20	33

The neutral environment is composed of the low-density neutral molecules in the upper edges of Earth's atmosphere that impact the spacecraft as it moves

through its orbit, decreasing effects as orbital altitude increases. The neutral environment can degrade spacecraft surfaces with atomic oxygen, reduce spacecraft lifetime or cause reentry due to atmospheric drag lowering its orbit, and affect constellation spacing due to differences in aerodynamic forces [1]. Micrometeoroids and orbital debris (MMOD) can collide with spacecraft and cause increasing damage with size, especially due to the high orbital velocity of the bodies. Over time, tiny collisions can degrade the spacecraft's structural components and solar panels or break off spacecraft components, creating more MMOD. The radiation environment is primarily caused by the Sun, including thermal and ionizing radiation, which vary with the level of solar activity. Radiation can also originate from Earth's albedo and intergalactic sources. The thermal environment caused by the Sun and orbital parameters drives the thermal design of a spacecraft. Ionizing radiation is primarily a concern for spacecraft electronics' radiation dosage and the potential for single event upsets [1]. Finally, the plasma environment is the generated energetic, ionized gases from interactions between gas particles and solar radiation. The plasma environment affects the heating and charging of a spacecraft, due to its high temperature and ionization. Interactions with plasma can affect the material choices of a spacecraft. These components of the space environment affect all subsystems on a spacecraft and must be taken into consideration during the design of the vehicle.

These environmental aspects can also combine to create synergistic effects on spacecraft, which can be more damaging than the sum of the parts. For example, a structure can be weakened by exposure to atomic oxygen, causing it to break off after an micrometeorite collision. The conditions found in space are generated from the environment naturally surrounding Earth, a spacecraft itself, or an interaction between the ambient environment and the spacecraft. The

magnitude of the observed effects from each component of the space environment therefore depends on the orbital location, the vehicle composition, and vehicle configuration.

1.2 Motivation and Objectives

The space environment generates many engineering challenges for spacecraft, particularly with synergistic effects that can magnify the harm produced by the environment. The effects of atomic oxygen (AO) on surface degradation of materials have been extensively studied [2]. However, there has been limited research on the effects of AO on structural properties of materials. Charles Ward conducted research at California Polytechnic State University, San Luis Obispo (Cal Poly SLO) to preliminarily characterize the effects of AO on the bending strength of carbon composite sandwich structures [3]. His primary focus was on the modification of a ground-based atomic oxygen simulation apparatus to accommodate the required three-dimensional samples for structural testing. He was able to research a test case using this apparatus with a limited scope. His thesis laid the groundwork to continue research in this area of space environmental effects. The research conducted for this thesis seeks to build on his test case of structural samples within the atomic oxygen simulation apparatus to better understand the effects of AO on structural material properties. Additionally, his research observed but did not characterize the generation of particulate from the AO-exposed carbon composite face sheets of the tested sandwich structures.

The objective of this thesis is to investigate the effects of AO exposure on carbon fiber and epoxy composite materials. It has been shown in previous research that AO has effects on some structural properties and the particulate contami-

nation generation of carbon composites. This research will specifically examine the short beam shear strength, percent mass loss, and particulate contamination resulting from carbon composites exposed to atomic oxygen. The short beam shear strength is a comparative property of material strength. The characterization of the percent mass loss and particulate contaminants will identify the risks of contamination generation on-orbit. The results of this research can then be used to better characterize the performance of carbon composites in space applications and inform their use.

Chapter 2

BACKGROUND

The background subjects for this thesis will be discussed in this chapter. The chapter begins with an examination of atomic oxygen and its effects on materials. The ground-based simulations for atomic oxygen will then be explored. Existing research on the effects of AO on composite material properties will be reviewed. Finally, the implications of particulate contamination and its relation to AO will be investigated.

2.1 Atomic Oxygen and Its Effects

Atomic oxygen (AO) is generated when ultraviolet (UV) radiation interacts with oxygen molecules in the low-density upper atmosphere, primarily in altitudes between 175 and 600 km above Earth [1]. For this reason, it only significantly affects spacecraft near this range in Low Earth Orbit (LEO) since there is a high enough density of AO to generate a significant effect. Figure 2.1 shows the number densities of ambient gas constituents of the upper atmosphere by altitude as calculated by the Naval Research Laboratory Mass Spectrometer Incoherent Scatter model (NRLMSISE-00) [4]. Atomic oxygen can be seen to be the dominant species in altitudes from about 300 to 700 km. This range corresponds to a majority of the LEO regime and therefore becomes a significant environmental effect for designing spacecraft operating within these altitudes.

Atomic oxygen is generated through a process called photodissociation, where stable diatomic oxygen molecules (O_2) are separated into highly reactive singular oxygen atoms, called atomic oxygen (AO) [2]. Ultraviolet radiation, with

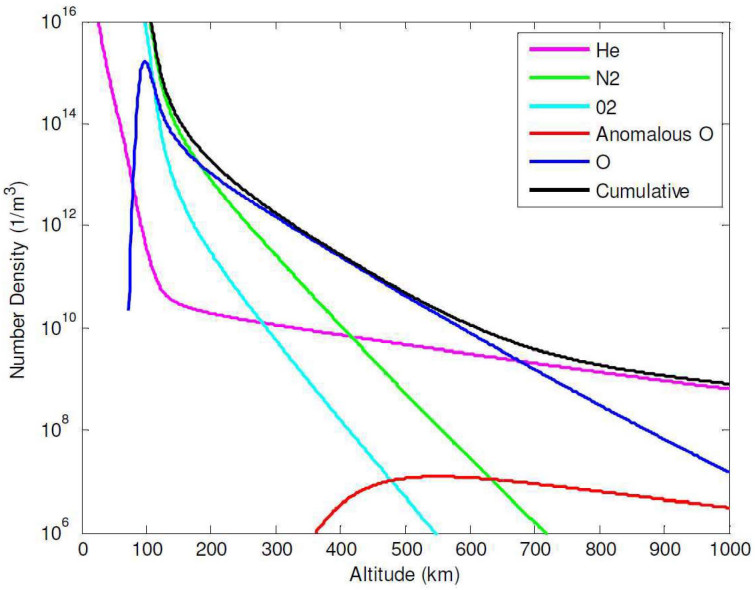

Figure 2.1: Number Density of Ambient Gases in Earth's Upper Atmosphere Based on NRLMSISE-00 Model [5]

wavelengths less than 243 nm, has enough energy to break the chemical bond of diatomic oxygen molecules; atomic oxygen therefore becomes the dominant ambient gas when this radiation reacts with oxygen molecules and the atmospheric density is too low for these atoms to recombine [2]. The amount of AO generated is also affected by solar activity, with more AO flux, or particles per unit area per unit time, present during high solar activity due to the increased radiation, and less during low solar activity. These AO particles can interact with spacecraft surfaces as part of the neutral environment of the spacecraft as it moves through the low-density atmosphere. Therefore, AO particles primarily affect spacecraft surfaces in the RAM direction, as the higher relative speed of the spacecraft causes collisions with particles in front of it. These impacts cause erosion on exposed surfaces due to their high impact speed combined with the high chemical reactivity of atomic oxygen. These collisions can induce overall mass loss either from the impact energy of the collision (about 5 eV) or the outgassing of produced volatile oxides after a chemical reaction with a surface material [2].

The chemical reactions caused by AO are most damaging when volatile oxides are produced. These oxides can then outgas from a spacecraft surface, with the potential to contaminate sensitive surfaces elsewhere on the spacecraft. Polymers are most likely to form volatile oxides after a chemical reaction, while most metals and silicones produce non-volatile oxides that can potentially shield lower layers from further interactions with atomic oxygen [2]. For this reason, AO-resistant coatings are generally used for polymers but are unnecessary for metal and silicone surfaces. However, AO can cause increased effects in the case of a phenomenon known as undercutting, which occurs at defects in protective coatings. Underneath such a material defect in a coating, AO will react with the underlying polymer and create a crater at the site of the defect. If the material is coated on both sides, AO can become trapped between the coatings and further erode the material with a higher reaction efficiency as shown in the Monte Carlo simulations of Figure 2.2 [2]. The effects of undercutting are able to structurally compromise the material, if the AO exposure is long enough to create significant cavities in the material.

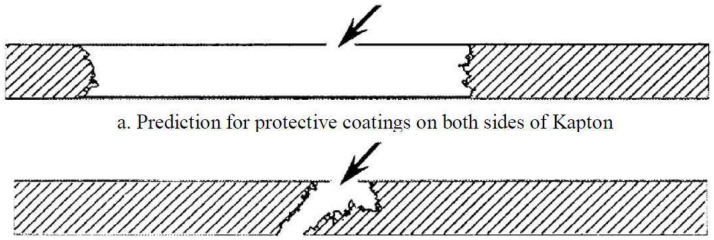

Figure 2.2: Monte Carlo Simulation of Erosion for Aluminum Protected Kapton [2]

The collision energy of AO can also cause erosion of spacecraft surfaces. While volatile oxides created by AO will outgas due to the vacuum environment, the collision of AO with products of previous chemical reactions will mechanically

remove molecules from the spacecraft surface. In the example shown in Fig. 2.3, the process of chemical bonding and physical removal is shown for a graphite surface. An impacting oxygen atom can bond with a surface carbon atom, given enough energy. If another oxygen atom impacts the bonded oxygen-carbon, the oxygen-carbon molecule will break away from the rest of the graphite structure. The weaker bonds due to the addition of oxygen to the molecular structure allow for particles to be eroded when more AO impacts the affected surface [2].

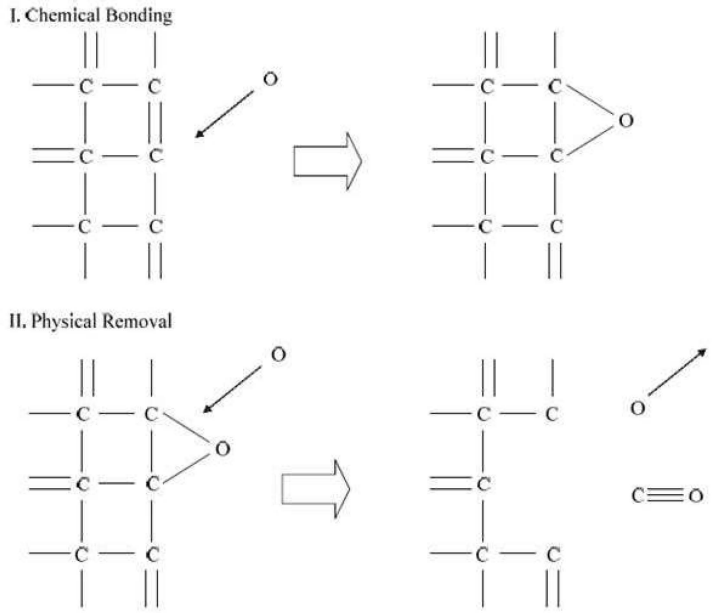

Figure 2.3: Atomic Oxygen Erosion of Example Graphite Surface [5]

Atomic oxygen is a serious consideration during spacecraft material selection for LEO missions. Volatile oxides can interact with other materials on a spacecraft or contaminate sensitive surfaces. The surface erosion can also change a material's mechanical, optical, and thermal properties, changing the overall performance of the spacecraft [6]. The damage caused by AO exposure, as well as its synergistic effects with vacuum and UV (VUV) environments, poses a formidable challenge for materials in the space environment.

2.2 Ground-Based Simulations of Atomic Oxygen

In order to understand how a material reacts in a given space environment, testing of the material must be conducted. This testing can occur on-orbit or using a ground-based simulation. It can be advantageous to test using a ground-based simulation because of the large costs associated with on-orbit testing due to spacecraft development and launch. However, ground-based simulations are not able to replicate every aspect of the space environment; therefore, better simulation chambers are developed in order to predict and evaluate environmental interactions and synergistic effects. These experimental results can then be incorporated into computer models for the space environment, used to qualify materials for use in space, or predict the performance of a material in a particular environment.

Ground-based AO simulation can be done by plasma ashers, continuous or pulsed lasers, gridded or gridless ion sources, or microwave electron cyclotron resonance sources. Plasma ashers use radio frequency (RF) energy to create thermal energy plasma, typically as a capacitively coupled plasma (CCP) or inductively coupled plasma (ICP) [7]. Their advantages include simplicity and lower cost, with the ability to provide large areas with high flux exposure. Lasers can be used to generate AO using a blast wave, which can be utilized at medium vacuum to generate a high flux, mono-energetic AO beam [5]. Ion sources use pure oxygen to produce very high energy AO with a limited flux [8]. Lastly, Electron Cyclotron Resonance (ECR) uses an induced magnetic field to generate AO in directed or isotropic beams at medium vacuum pressure [9]. Each type of system can be used to simulate the AO environment; however, they each include environmental differences from what is seen on-orbit. These differences in vacuum pressure, directionality, kinetic energy, and flux affect how well the generated AO

can replicate the space environment in a ground-based system.

In order to standardize methods to reliably compare data across ground-based AO erosion facilities, ASTM E2089 was created [10]. The document includes standard operating procedures and calculation methods for the AO fluence of the test. It also defines the four recommended witness materials for determining the AO flux and fluence: Kapton polyimide (H or HN), TFE fluorocarbon fluorinated ethylene propylene (FEP), low density polyethylene, and pyrolytic graphite [10]. The standard also outlines the requirements for proper vacuum dehydration and subsequent sample weighing; samples should outgas for a minimum of 48 hours at or below 200 mTorr and be weighed within 5 minutes of removal from vacuum. These steps reduce uncertainties due to the reabsorption of vapors when the samples are removed from vacuum. Finally, the standard includes recommendations for sample preparation, handling, and sizing. This standard allows for better comparisons between the data found at different facilities, regardless of the type of AO simulation method they use.

This research used a CCP plasma asher for environmental testing. Plasma ashers generate isotropic AO, whereas orbital environments receive either directed or sweeping RAM atomic oxygen [7]. The isotropic AO does not create the same pits and cones in surface texture as seen on-orbit due to this difference in kinetic energy: plasma asher AO has a kinetic energy of $\approx$0.04 eV and LEO AO has a kinetic energy of 4.5 eV [7]. However, a higher concentration of thermal energy AO plasma is generated inside a plasma asher to achieve comparable levels of oxidation to on-orbit. Other environmental differences from on-orbit conditions include the total radiation environment and neutral particle concentrations. Ground-based AO simulations are useful to determining the effects on materials, but the applicability of their results must also account for the

differences in environment between the simulation chamber and on-orbit.

2.3 Mechanical Testing of Atomic Oxygen Exposed Materials

Mechanical testing of atomic oxygen exposed materials is meant for situations of structural stress on-orbit. Micrometeoroids and orbital debris (MMOD) can impact spacecraft in LEO at speeds on the order of km/s [1]. Spacecraft are also exposed to thermal cycling during orbit, which can especially affect large, rigid, deployable solar panels. These cases are examples of structurally stressful environments while the spacecraft is exposed to atomic oxygen.

Carbon composites are a suitable material for shielding against MMOD impacts. Their fiber and matrix structure creates a higher specific energy absorption in a hypervelocity impact than aluminum alloys, which are typically used in conventional Whipple shields [11]. However, when comparing the performance of composite shields with and without exposure to AO and UV radiation, unexposed samples were found to absorb more impact energy [11]. The outgassing due to vacuum and the erosion due to AO degraded the mechanical properties of the carbon composites, reducing their expected performance on-orbit.

Due to their high strength, high stiffness, low weight, near-zero coefficients of thermal expansion, and dimensional stability, advanced carbon composites are well-suited to spacecraft applications [12]. Thermal cycling is seen constantly by most spacecraft structures in LEO due to the short orbital periods, passing from sunlight to shadow multiple times a day. Therefore, carbon composites for LEO applications require thermal durability over a satellite's lifetime. A study found that thermal cycling of unidirectional carbon fiber and epoxy composites decreased the ultimate strength, elastic modulus, interlaminar shear strength,

flexure properties, and longitudinal properties [12]. More research on graphite epoxy composites in AO and LEO synergistic environments also found a decrease in tensile strength and stiffness compared to a baseline [6]. The AO-exposure degraded the composite's performance, and the addition of thermal cycling and UV radiation further decreased the composite's strength [6]. Therefore, the thermal durability of carbon composites must be taken into account when designing for LEO satellites, which can be further reduced by exposure to AO as the epoxy matrix is eroded.

Four-point bending tests on AO-exposed samples was conducted by Charles Ward at Cal Poly SLO [3]. As a test case for the modified MAX chamber, carbon composite and aluminum honeycomb sandwich structures were exposed to AO and tested in four-point bending. It was found that the exposure to AO weakened the samples; however, the sample size was limited to 22 and the analysis was performed as a pair study due to inconsistencies in manufacturing. Samples of similar material, manufacturing process, and defects were paired and the difference in the slope of the linear portion of the stress-strain curve of the pair was compared [3]. Existing research on effects of space environments, such as AO exposure, UV radiation, and thermal cycling, on carbon composites demonstrates a degradation in their material properties.

2.4 Atomic Oxygen and Spacecraft Contamination

When designing spacecraft, contamination from the selected space environments must be taken into account over the course of the spacecraft's operation. Contamination can come in two forms: molecular and particulate, both of which can be found on the ground and on-orbit. Molecular contamination is defined

as being undesired foreign film matter without definite direction [13]. Particulate contamination is categorized as being small undesired foreign material with observable dimensions, generally on the order of micrometers or larger [13]. On orbit, particulate contamination can be caused by surface particles, plume products, ice formation, mechanism generated particles, MMOD, and extravehicular activity [14]. These environmental effects in space can magnify the effects of a source of contamination, both individually and synergistically.

When particulate contamination is on a spacecraft, it affects sensitive surfaces either through surface obscuration or scattering. For reflecting surfaces such as mirrors in optical elements or thermal control surfaces, particulate change the surface's absorptivity [13]. Pariculate will absorb light rather than reflect it on a mirror; similarly, the absorption of light by particulate on a thermal control surface will change the net effective solar absorptance or emissivity. Particulate also negatively affects transmitting surfaces, such as solar arrays, lenses, focal plane arrays, and concentrated optics. On a solar array, surface obscuration by particulate creates a power degradation. Particulate reduces signal strength of transmitting optical elements, which is particularly damaging due to the concentration of light on these surfaces from a primary reflecting mirror [13]. Scattering is a product of light reflecting off of particulate. This can be damaging to a spacecraft's mission if the particulate is collected on an absorptive surface, such as a baffle. Elements in an optical train or sensor that are meant to be shielded from stray light will receive the incident light from the particulate, either overwhelming the signal from the intended target or damaging the focal plane [13].

Atomic oxygen can cause contamination as it erodes a surface or creates volatile materials that can then be outgassed from an exposed surface. Atomic oxygen erosion creates the potential for contamination as particles are either

mechanically removed or volatile oxides are created. These particles can then be transported to a more sensitive spacecraft surface to degrade the satellite's overall mission performance over time. Sensitive instruments are most at risk to surfaces within their field of view; large surface areas, such as solar panels, are most likely to generate contamination. The particulate generated from atomic oxygen can potentially be transported to a sensitive surface either through outgassing or after an MMOD impact [13].

In the research conducted by Charles Ward, particulate contamination due to AO was coincidentally found [3]. When preparing samples for structural testing, a black residue could be easily wiped from the exposed surface with a Kimtech wipe as shown in Fig. 2.4. However, the nature of the erosion was only observed and not investigated in his research. The presence of particulate contamination due to AO-exposure is an important observation, since carbon composites are generally used for structural components of solar panels, and therefore have large surface areas.

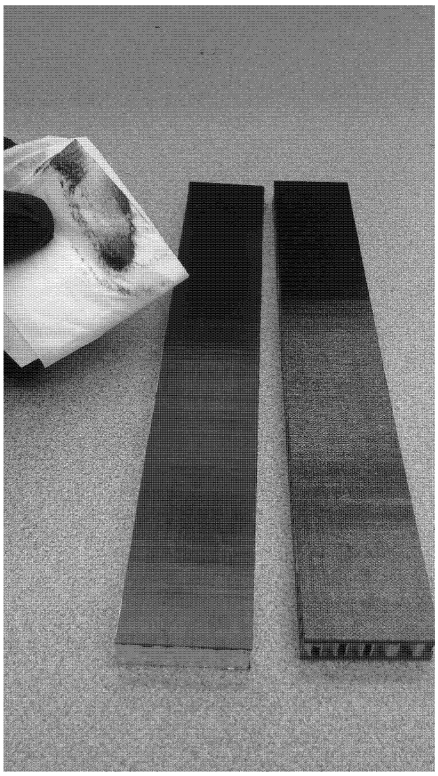

Figure 2.4: Residue from Composite after AO Exposure [3]

Chapter 3

EXPERIMENTAL APPARATUS

This chapter will describe the experimental apparatus used in this work, starting with the AO simulation chamber MAX. It will describe the desiccator used for sample bakeout and the autoclave used for curing the samples. The chapter will conclude with the measurement systems used throughout experimental environmental, contamination, and mechanical testing.

3.1 Atomic Oxygen Simulation Chamber

The Aerospace Engineering Department at Cal Poly SLO operates an atomic oxygen simulation vacuum chamber, commonly referred to as MAX. This chamber was initially refurbished by Max Glicklin, who designed the original AO generation system configuration for the retrofitted Veeco Model 747 deposition chamber [5]. The original system was a capacitively coupled plasma (CCP) system including a radio frequency (RF) generator, load matching network, system controller, two parallel electrodes, and a thin sample grounding and cover plate [5]. The simulation chamber within the Space Environments Lab is pictured in Fig. 3.1.

The chamber's CCP system is powered by a Seren R301 MKII power generator manufactured by Seren Industrial Power Systems operating at 13.56 MHz. An attached AT3 impedance matching network is included as protection for the radio frequency (RF) generator from internal damage from reflected RF power. These systems are both controlled by a Seren MC2 controller, which adjusts the variable capacitors of the AT3 matchbox [5]. These components are stored on the shelving unit next to the chamber. The chamber uses a 50 cm diameter by 32 cm tall

Figure 3.1: MAX AO Simulation Chamber Setup

Pyrex cylinder to enclose the sample testing setup. Additionally, there is a needle valve to allow in adequate air to generate atomic oxygen. The chamber uses an Adixen ACP 28 pump by Pfeiffer Vacuum, with a maximum pumping speed of 28 m^3/hr. A schematic of the vacuum chamber and its components is displayed in Fig. 3.2.

In Fig. 3.3, the original plate configuration and sample securing apparatus is shown. This configuration was used to test thin films and could include a VUV lamp for testing synergistic interactions with AO exposure. The configuration could be used to test at most four thin film samples at a time. The film samples were held between a base plate and face plate, exposing a circular area to the atomic oxygen. The electrode plates were optimally separated by 7.62 cm [5]. Exposure between experimental samples was compared using the fluence of AO,

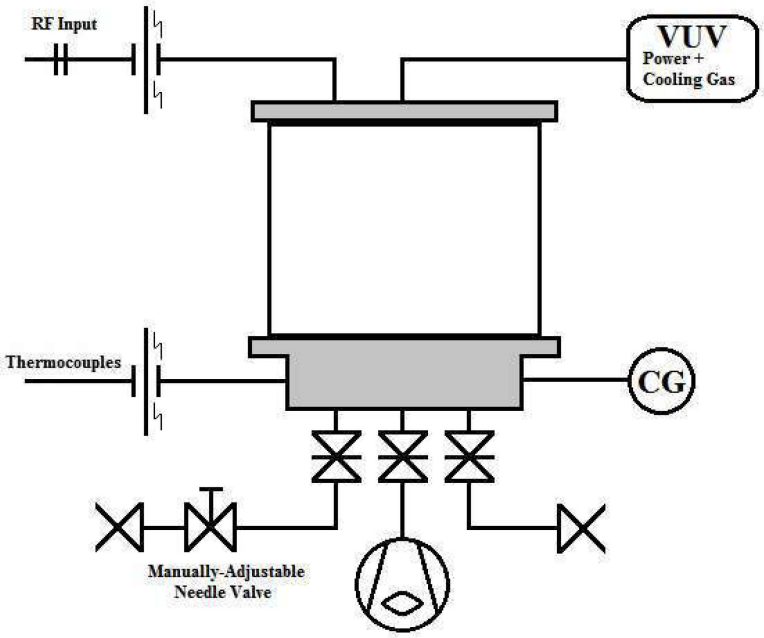

Figure 3.2: MAX Chamber Vacuum Schematic [3]

which was determined based on the mass loss of a witness sample (generally Kapton polyimide film) with a fixed exposed surface area as discussed in Section 6.1. More information about the chamber's original configuration and components can be found in Max Glicklin's thesis [5].

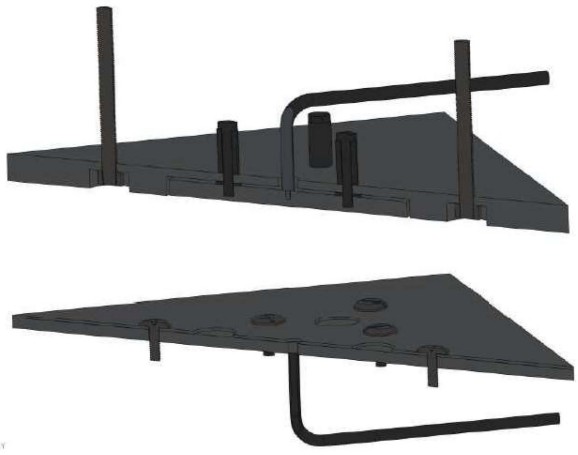

Figure 3.3: Original Configuration of MAX Chamber [5]

The MAX chamber underwent further modification with the work of Charles Ward to accommodate three dimensional samples [3]. The lower assembly was adjusted so that different base plates could be mounted for either thin or three-dimensional samples, while keeping the distance between the electrodes constant [3]. The new system configuration allows for the original testing configuration of 4 thin samples or 2 rectangular troughs for three-dimensional samples with space for a witness sample. The gap distance between electrode plates remained at 7.62 cm. Figure 3.4 shows the new face plate design for three-dimensional samples. However, it can be seen that there is no designated area for the necessary witness sample. The witness sample must be secured on an available space on the face plate where it will be exposed to the atomic oxygen. More information about the changes to the testing assembly can be found in Charles Ward's thesis [3]. With this augmentation to the MAX chamber, AO-exposed three-dimensional samples can then be stress tested using the Aerospace Engineering Structures and Composites Lab to investigate environmental effects. This research utilized the two-slot face plate for the three-dimensional test samples.

When the AO simulation chamber was constructed, an optimal operating procedure was developed for AO generation. The RF power generator is set to 125 W and the pressure of the chamber is kept at 175 $\pm$ 10 mTorr. During operation, the chamber pressure and RF phase and magnitude is monitored. The chamber during use is shown in Fig. 3.5. These operational parameters generate the expected thermally energetic, non-directional AO that has been characterized for this system. The exact procedure for the chamber's operation is included in Appendix B.

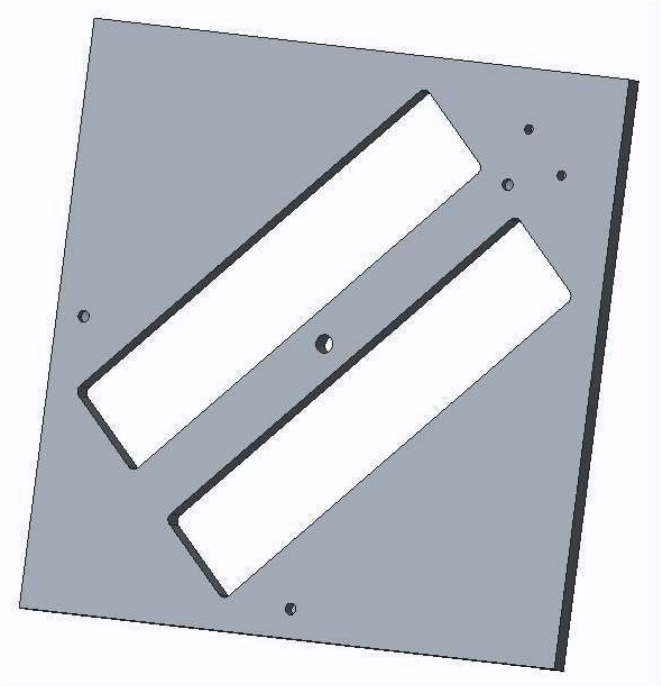

Figure 3.4: Three-Dimensional Face Plate [3]

Figure 3.5: Samples in MAX Chamber with Atomic Oxygen

3.2 Desiccator

According to ASTM E2089, a 48-hour dehydration process is required before samples are exposed in the AO chamber. The Kartell model DYNCR 243065 desiccator, known as Junior, was used for this purpose over the course of experimental testing. Junior is a large plastic, circular desiccant chamber with a clear lid, whose schematic is depicted in Fig. 3.6. It uses a Two Stage Rotary Vane pump from Cacejen Vacuum that operates at 15.2 ft^3/min. A dedicated desiccator for experiments in MAX is necessary due to the increasing demands within the Space Environments Lab from graduate research and undergraduate lab courses. The separate desiccant chamber could be used regardless of other lab activities, especially since it is stored on a cart.

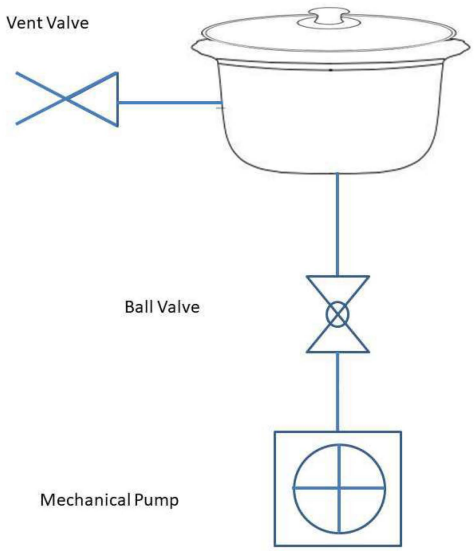

Figure 3.6: Junior Chamber Schematic [3]

This desiccator was adequate for this work because many samples could be stored in Junior at once. The samples could be stored along the outer rim or on the base of the container, as shown in Fig. 3.7. Additionally, it was analyzed

to have reached the required levels of vacuum (on the order of 100 mTorr) comparable to MAX during AO use [3]. The chamber was used for initial sample bakeout and control sample storage under vacuum during sample AO exposure. The entire setup of Junior with its dessicator, pump, and cart is shown in Fig. 3.8.

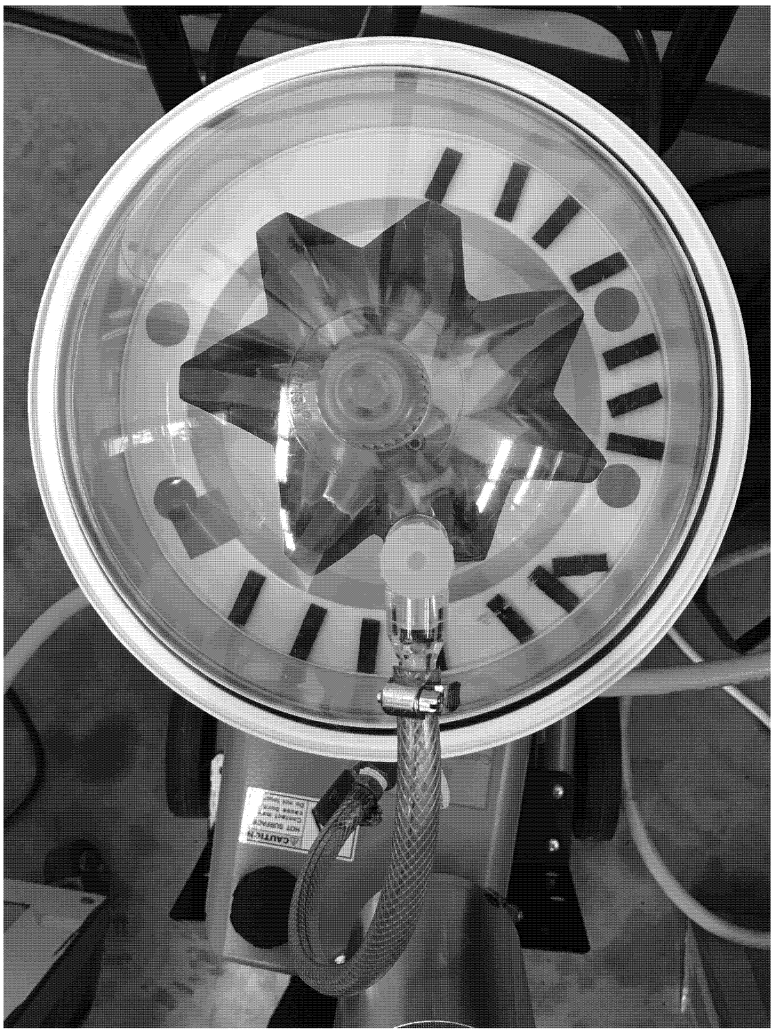

Figure 3.7: Sample Bakeout in Desiccator Junior

Figure 3.8: Junior and Cart Setup

3.3 Autoclave

In order to cure the carbon fiber composite prepreg as further described in section 4.2, the autoclave in Fig. 3.9 from the Structures and Composites Lab was used. Pressure and heat are generally required to cure composites with resin. The pressure from an autoclave is used to remove air bubbles from layers in a laminate and squeeze out excess resin. The autoclave is able to cure the composites by controlling the pressure and temperature within its pressurized hollow shell. The autoclave used is able to reach temperatures of 538°C and pressures of 6.9 bar. The composite is placed on a plate and sealed to create a vacuum while connected to a pump inside the autoclave.

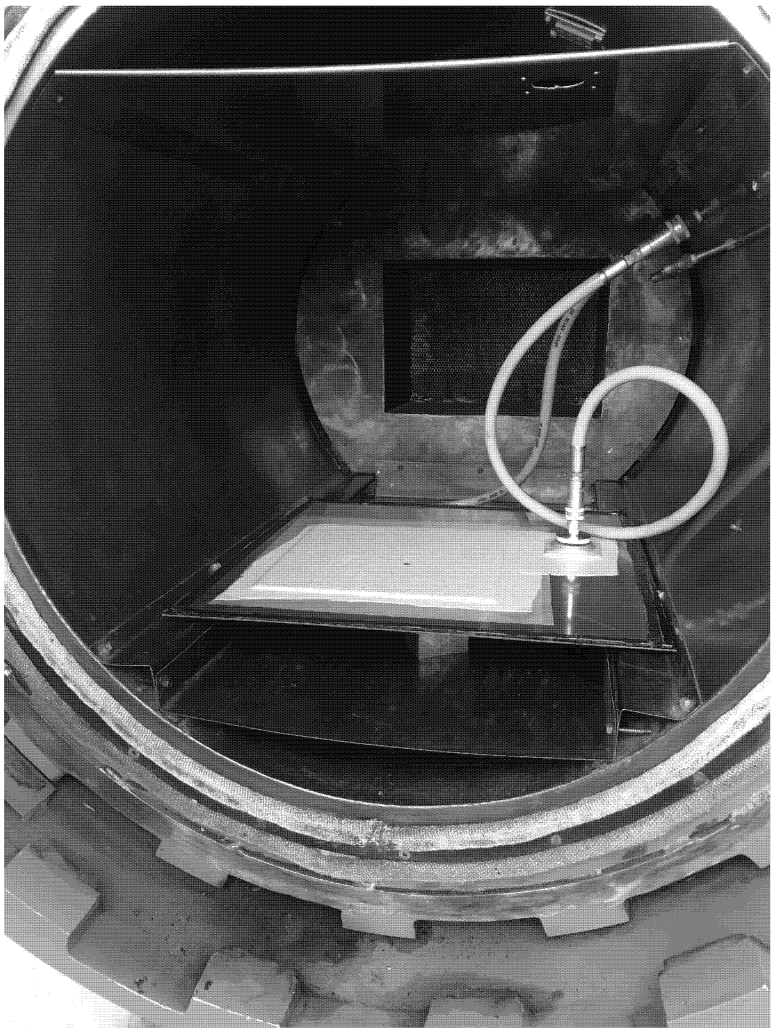

Figure 3.9: Autoclave with Laminate Prepared for Curing

3.4 Instron Mechanical Testing Machine

For structural testing, force and position measurements were collected from a 5960 Series Dual Column Tabletop Instron mechanical testing machine. The data is recorded through an internal data acquisition (DAQ) system as it is measured by a 50 kN 2580 series static load cell. The data is then processed using the Instron Bluehill software and can be exported to a CSV file for further analysis of the collected measurements. This software is also used to program the testing

procedure for the Instron machine. During testing, it displays the collected data in real time as well as previously collected data within the testing session. The Instron machine is shown in Fig. 3.10.

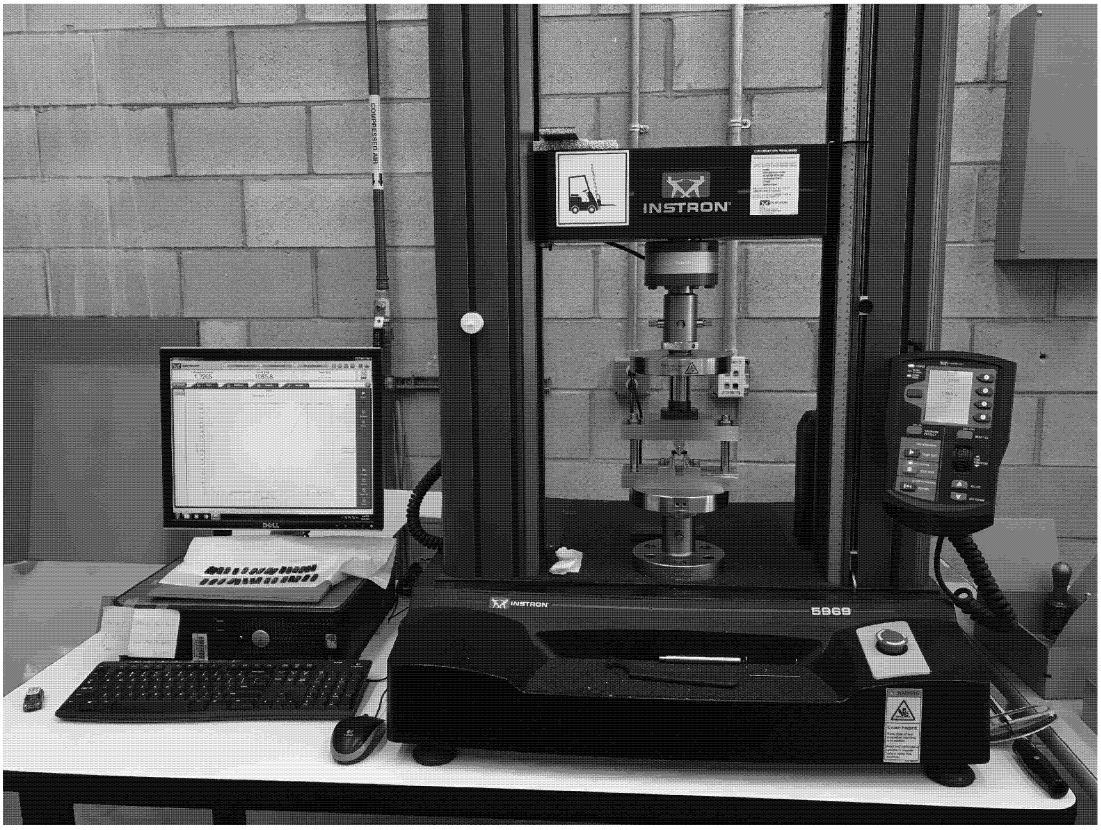

Figure 3.10: Instron Mechanical Testing Machine with DAQ System

The upper crosshead and base adapter are equipped with the fixtures for a short beam shear test, although other setups can be used for other kinds of mechanical tests. During testing, the crosshead and attached fixture can be raised or lowered at a constant rate determined by the chosen testing procedure. The base adaptor and fixture remain stationary; in the short beam shear test, they support the sample as the crosshead is lowered.

3.5 Measurement Systems

For each sample, basic measurements of size and weight were required. Calipers with a readability of 0.01 mm were used to measure the length, width, and thickness of each sample. The sample dimensions were required in order to calculate the material parameter of short beam shear strength from the structural testing. A VeriTas S-Series precision balance was used to measure mass. This balance had a readability of 0.001 g and a repeatability of 0.0005 g [15]. The mass was necessary in order to track mass loss over the dehydration and AO-exposure.

Particulate contamination was collected using Teflon tape lifts in a process further described in Section 5.2 based on ASTM E1216. The Teflon tape used for the tape lifts was chosen because it does not pull up fibers from carbon composites, which the suggested tapes outlined in ASTM E1216 would do. The Teflon tape used was graciously donated from NASA Jet Propulsion Laboratory.

To measure the particulate contamination, a Leica DM IRM microscope from the Materials Engineering Metallography Lab at Cal Poly SLO was used to image the tape lifts. The microscope, shown in Fig. 3.11, interfaced with the QCapture Pro software, which was used to capture high resolution images of the magnified view. Each tape lift was imaged 30 times, in a 3×10 grid at 100x magnification. This is visualized in Fig. 3.12, with images being taken at the black squares at the points of the red grid. Each sample imaged had a tape lift from before and after AO exposure, so each sample imaged generated 60 images.

The images were then processed using the open source software imageJ to determine percent area coverage (PAC). The dark particulate and fibers contrasted with the light Teflon tape, which was used to choose a gradient threshold to sort the pixels of the image. The PAC was the percentage of the number of dark

Figure 3.11: Leica DM IRM Microscope

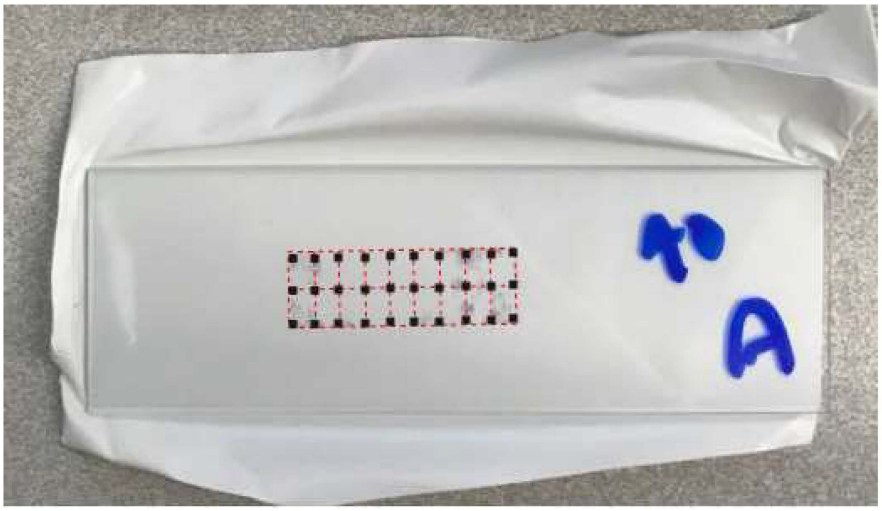

Figure 3.12: Visualization of Image Grid on Tape Lift

pixels within the chosen threshold per the total pixels in the image. In order to calculate this parameter, each image was converted to grayscale and the contrast

was increased. A threshold of darkness was chosen by the experimenter for every image to capture the most particulate and least amount of shadow on the tape lift. The software would then analyze the image to determine the percentage of pixels within that selected threshold, as shown in Fig. 3.13. A threshold of color values was chosen for a grayscale image to encompass the area covered by carbon fiber particulate, highlighted in red against the grayscale image in the figure below; however, not all of the particulate is included and some shadow is included in the bottom left corner. This process is further described in Section 6.4.

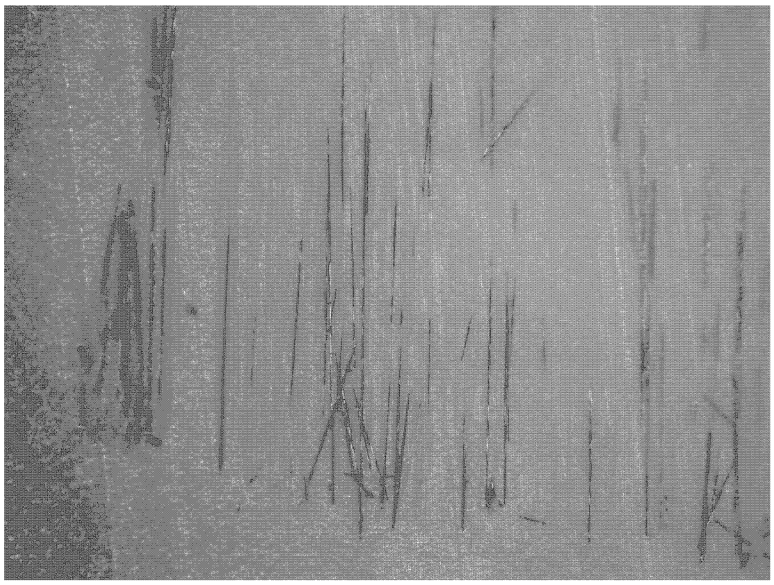

Figure 3.13: Tape Lift Image with Highlighted Threshold

This process was also used to estimate the irregular exposure area of the Kapton film witness samples. Since the two slot face plate does not have a designated witness sample location, there were irregular exposure areas for the Kapton film witness samples per test. A scale was defined within each image by including a ruler in the image. The ruler and background were then removed from the image. A threshold was chosen to encompass the discolored exposure

area and particle analysis was conducted as with the microscope contamination images to calculate the exposure area. Similarly to the tape lift procedure, the experimenter chose an appropriate threshold that encompassed the most exposure area and least unexposed area. This process and its implications are further discussed in Section 7.1.

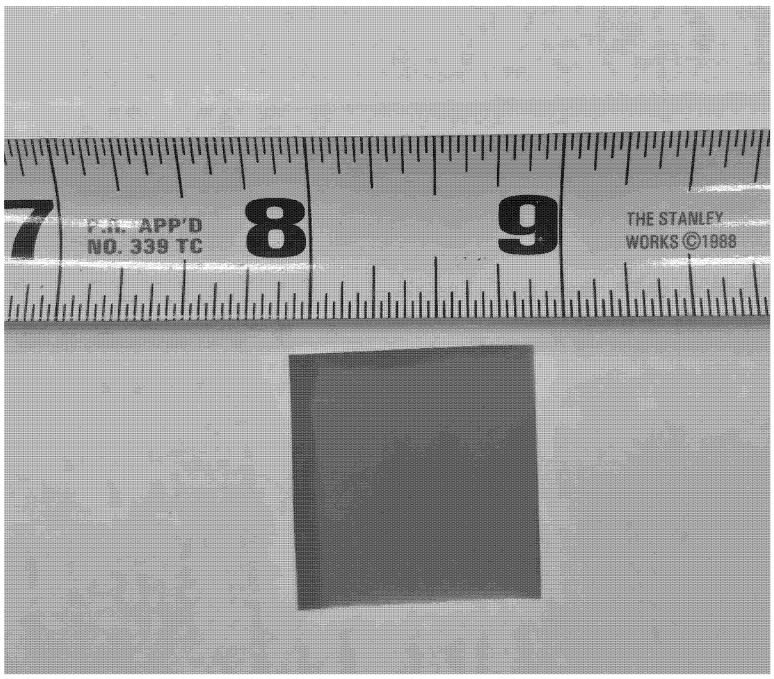

Figure 3.14: Exposed Kapton with Ruler Scale

Chapter 4

SPECIMEN PREPARATION

This chapter follows the sample preparation process, which was completed twice over the course of experimentation. The material used is introduced, followed by the procedure for sample fabrication. Finally, the finished specimens are summarized to illustrate the slight variations between samples.

4.1 Material

A carbon fiber and epoxy composite material was chosen for experimentation because of its widespread use in space applications due to its high strength-to-weight ratio and dimensional stability. The carbon composite samples were manufactured from RS-36 M55JB 6K UD, a space-grade unidirectional carbon fiber and epoxy composite prepreg that was graciously donated by TenCate Advanced Composites last year for Charles Ward's research. This material is often used for solar arrays [16] in space applications. The properties of the TenCate prepreg are shown in Table 4.1.

Table 4.1: TenCate RS-36 M55JB 6K UD Properties (Room Temperature Dry) [17]

Tensile Strength	2041 MPa
Tensile Modulus	313 GPa
Compressive Strength	993 MPa
Compressive Modulus	294 GPa
Interlaminar Shear Strength	75 MPa
Ply Thickness	0.06 mm
Outgassing	0.4% TML

It was found in previous research that carbon fiber and aluminum honeycomb

composite sandwich structures were thick enough (approximately 1.13cm) to have AO erosion on the sides [3]. Choosing a purely carbon fiber composite sample that was thinner reduced these effects and still reflected space applications of carbon composite structures. Additionally, the samples were simpler to manufacture so more samples could be produced than in the previous research conducted by Charles Ward. The same material was used for all sample fabrication to reduce variations seen in the samples.

4.2 Sheet Fabrication

The process of fabricating the samples started with cutting sheets of ply from a large spool of material. These sheets were then laid up in the appropriate geometry to have the desired sample thickness of 4 mm, corresponding to 53 layers of carbon fiber composite prepreg. This layer count for the desired thickness was estimated from the layup pattern and resulting sheet thickness from the previous research at Cal Poly SLO using this material [3]. The desired thickness was derived from the dimensional ratios for testing specimens given by ASTM D2344 [18] and the minimum span length required for the mechanical testing fixture. A 0-90 cross ply pattern was chosen for simplicity of fabrication as well as reduced vulnerability of the purely unidirectional layers. The outer layers were each 0-degree ply, with each layer alternating in orientation. Since there was an odd number of layers, the cross-ply pattern was balanced.

The process of cutting plies required consistency to get square sheets of the same size. The width of the prepreg material spool limited the size of the sheet to one square foot. Due to the required sample thickness and large number of layers, the composite sheet was laid up into sets of approximately ten layers that

were then put together. The tools used to cut the sheets are shown in Fig. 4.1 and the tools used to lay up the sheets are shown in Fig. 4.2. Each of the sets were carefully laid up to ensure square sides before they were all put together. Initially, one sheet was manufactured and generated 52 usable samples. After analysis of the results from these samples, it was determined that a second sheet should be manufactured. This enabled the experimenter to try to reduce the variation in mechanical testing results seen from the first few sets of samples, as well as supply enough samples to include 48-hour exposure tests.

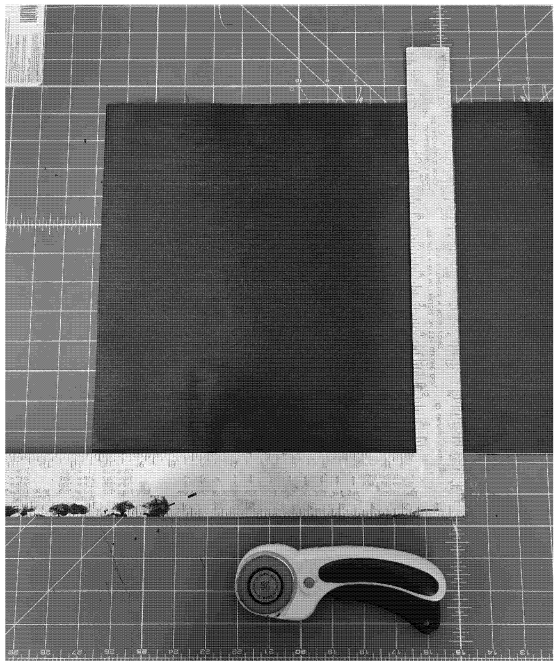

Figure 4.1: Tools Used for Cutting Plies

The autoclave from Cal Poly SLO Aerospace Engineering Department's Structures and Composites Laboratory was used to cure the composite sheets. The cure cycle is shown in Fig. 4.3, and was completed in the autoclave to the prescribed temperature and pressure profile [17]. The autoclave is capable of following the optimally prescribed temperature, pressure, and time for the composite material which reduced the potential for variation between sheets versus other curing

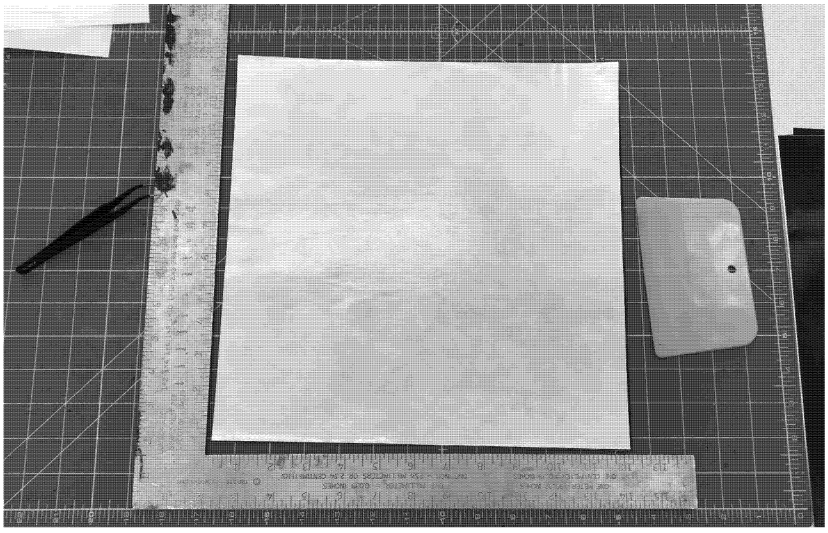

Figure 4.2: Tools Used for Laying Up Plies

methods. During curing, the bottom face of the laminate remained flat, while the top face sloped down at the edges. The top face additionally was more textured than the bottom face. The thickness of the sheet after curing was not exactly 4 mm, but ranged from 3.68 mm to 3.98 mm. The mean thickness was 3.82 mm with a standard deviation of 0.06 mm. This range in thickness was accepted by the experimenter to be adequate for testing since the samples also tended to be shorter in length and smaller in width, retaining the desired dimensional ratios.

4.3 Beam Specimens

After the sheet was cured, two steps were required to cut the sheet into the small short beam shear samples. The sheet was first cut into long strips of the desired 8 mm width by the water jet at Cal Poly SLO, shown in Fig. 4.4. These long strips were then cut using the tile saw in the Structures and Composites lab.

The water jet was used to cut the long strips due to its precision and speed. Each sheet fabricated was able to yield 20 strips that could then be cut into at

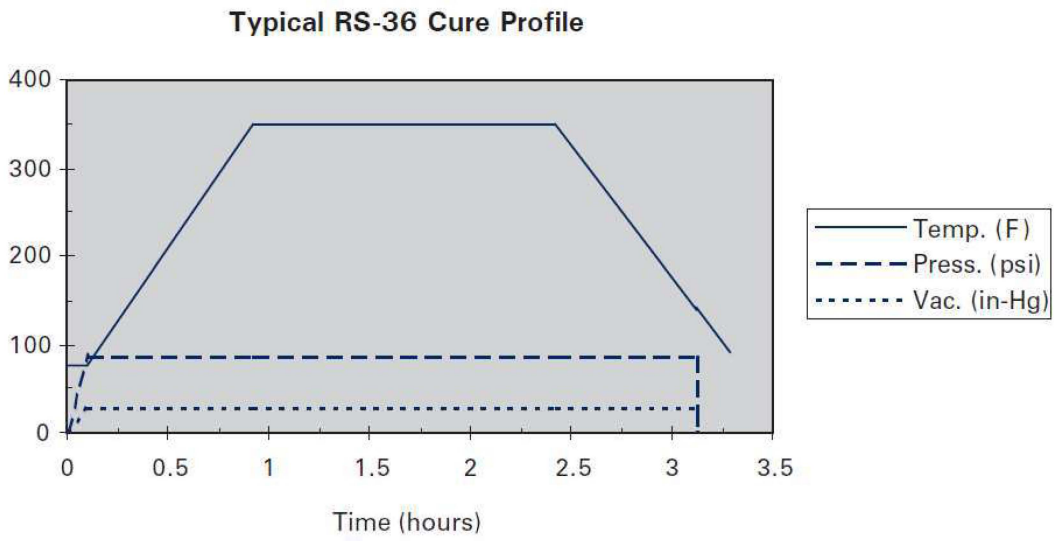

Figure 4.3: TenCate Prepreg Cure Cycle [17]

Figure 4.4: Water Jet Cutting Laminate

most 9 specimens. A two-dimensional rectangular specimen shape was drawn and saved as a .DXF file to be analyzed and used by the water jet's computer-aided manufacturing (CAM) software. The rectangular shape from the .DXF file was duplicated into a pattern using the CAM software. The water jet operating technician then aligned the water jet head with the composite sheet and ensured that the pattern fit within the dimensions of the composite sheet. The water jet cut the material using a mixture of high pressure water and grainy abrasive material. Each strip was cut individually, with the technician pausing the water jet in between. Each strip was removed after it was cut out during this pause to avoid any accidental damage from the water jet's stream. The composite sheet was held in place using clamps on two opposite sides, with the flat side resting on the supports. The excess material after the strips were cut could then be discarded.

Since the sheets were relatively thin, the force of the water jet's stream caused them to bend as more strips were removed, affecting the width of each strip. Strips cut from the middle of the sheet had an edge that was cut at a slight angle, reducing the width on one end. These affected strips only had samples cut from sections with straight sides and width of 8.00 ± 0.50 mm. The width of the samples ranged from 8.39 mm to 7.57 mm, with a mean of 7.78 mm and standard deviation of 0.19 mm. Additionally, the water jet cutting process caused some delamination along the edges of the top face of the strip. Both faces were tested over the course of this research and no noticeable difference was measured.

Each sample had to be cut by hand using the tile saw shown in Fig. 4.5. The ideal final samples would be 4.00 mm $\times$ 8.00 mm $\times$ 24.00 mm. The required length, as shown in Fig. 4.7, was marked in pen before being cut by the tile saw. Samples were only used if the length fell within 24.00 ± 0.25 mm, greatly

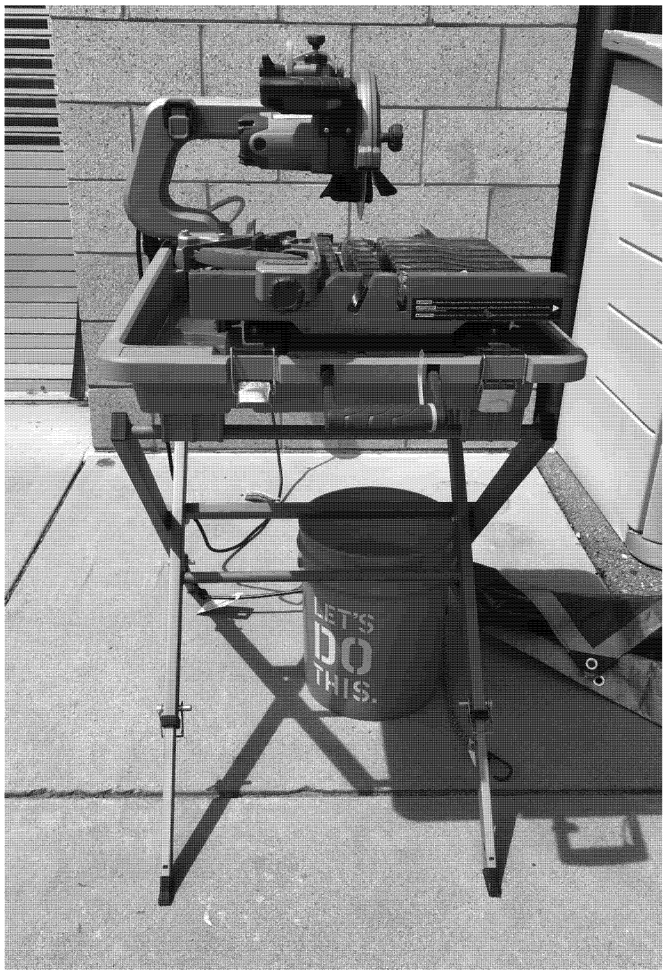

Figure 4.5: Structures and Composites Lab Tile Saw

reducing the number of usable samples during the start of testing. This was due to the imprecise alignment of each cut, which had to be approximated by eye using the edges of the saw and the marked length on the sample as shown in Fig. 4.6. The tile saw caused small amounts of delamination at the edges of the samples, and occasionally produced slightly angled end faces. This likely caused greater particulate generation at the sample ends but was not likely a factor in the mechanical testing results. The tile saw was chosen since it provided adequate accuracy with more availability for use than the water jet. Additionally, there were concerns about using the water jet for the small samples because the

composite samples are light enough to float on water and were more likely to be damaged by the water jet stream by an experimenter's error or the bending of the sheet.

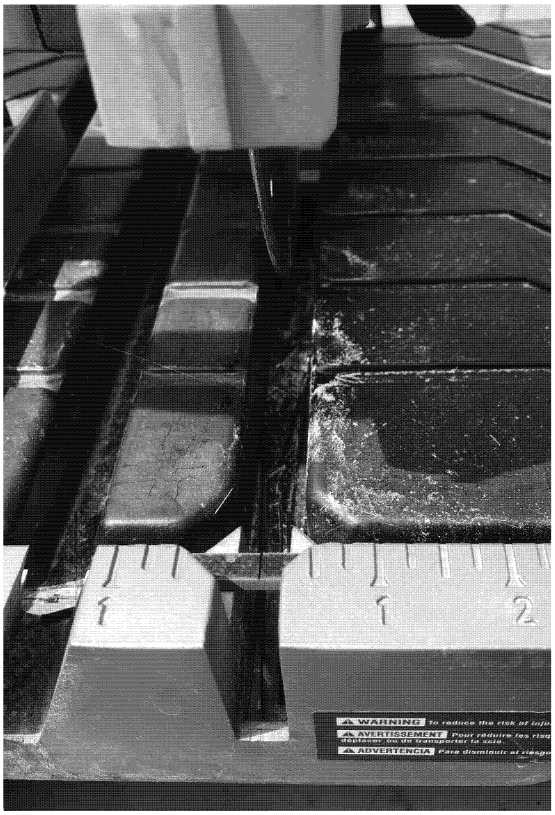

Figure 4.6: Tile Saw Alignment with Sample

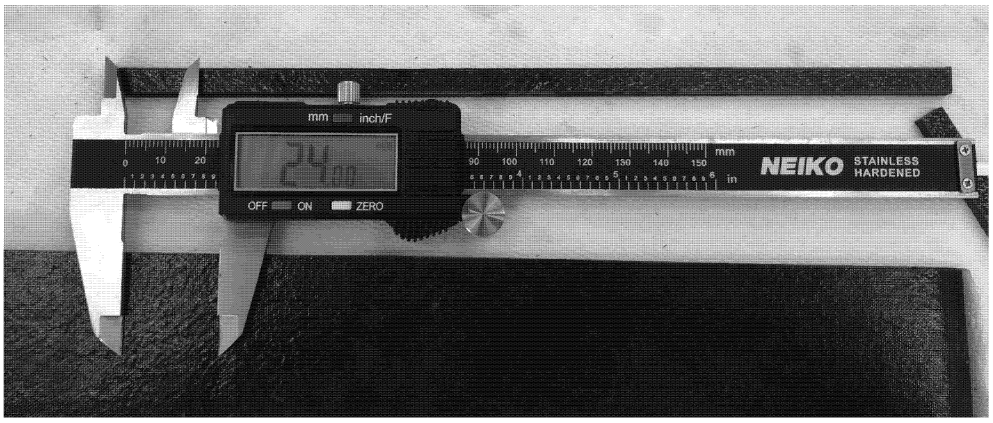

Figure 4.7: Measurement of Sample Length on Water Jet Cut Strip

4.4 Finished Samples

In total, 160 usable samples were fabricated for experimentation. Once fabrication was complete, finished samples were weighed using the VeriTas precision balance and measured with calipers before experimentation. Great care was taken to preserve numbering of samples without explicit labels attached to the specimens. Generally, they remained in their sample order and pictures were taken of their configurations within the experimental chambers to catalog their placement. It was found that two composite sheets were adequate to generate the 160 samples tested during this research. Due to their small size and ease of manufacture, many samples were able to be tested to explore the relationship between their material properties and AO exposure.

Table 4.2: Descriptive Statistics of Sample Physical Properties

	Mean	Standard Deviation	Maximum	Minimum
Length (mm)	23.97	0.14	24.25	23.75
Width (mm)	7.78	0.19	8.39	7.57
Thickness (mm)	3.82	0.06	3.98	3.68
Initial Mass (g)	1.073	0.041	1.170	1.017

The completed samples were numbered in order of manufacture and split into tests by the set of samples that went through environmental, contamination, and mechanical testing together, shown in Table 4.3. Tests 1 through 5 (103 samples) had a 24-hour environmental testing duration, and Tests 6 and 7 (57 samples) had 48-hour environmental testing duration. The first sheet supplied samples for Tests 1 through 3 (52 samples) and the second sheet for Tests 4 through 7 (108 samples). This increase in usable samples is due to the improvement of the experimenter's accuracy in using the tile saw. Contamination testing was conducted for the 24-hour AO-exposed samples from Tests 2 through 5 (48 samples), as will be

described in Section 5.2, and was limited to these tests by the amount of tape acquired.

Table 4.3: Distribution of Samples Among Tests

Test	Total	AO-Exposed	Control	Duration	Contamination Test
1	8	4	4	24hr	No
2	14	7	7	24hr	Yes
3	30	15	15	24hr	Yes
4	26	13	13	24hr	Yes
5	25	13	12	24hr	Yes
6	25	12	13	48hr	No
7	32	16	16	48hr	No

Chapter 5

EXPERIMENTAL TESTING

In this chapter, the steps for contamination and mechanical testing will be discussed. First, the procedure for AO environmental testing will be examined. Then the process for particulate contamination testing and short beam shear mechanical testing will be explored. The overall testing process is depicted in Fig. 5.1 below.

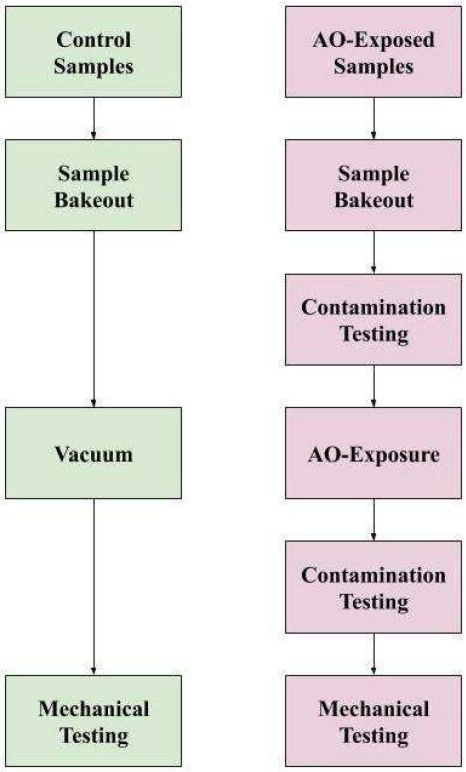

Figure 5.1: Sample Testing Process

5.1 Atomic Oxygen Environmental Testing

For each test, the samples were equally divided between treatments: AO-exposure and control. The AO-exposed samples underwent a procedure similar to ASTM E2089 as outlined in Section 2.2. The control samples would remain under vacuum in the desiccator Junior. All samples would outgas in a 48-hour bakeout in Junior before treatment. After the 48-hour mark, all samples were removed and weighed using VeriTas precision balance before they were divided into their treatment. Since the samples were small enough, 48-hour bakeouts were sufficient to fully outgas the samples. Control samples showed little to no change in mass after being put into vacuum again after a 48-hour bakeout, as will be shown in Section 7.2.

The samples were assigned a treatment such that there were roughly equal amounts of samples of similar size within each treatment group. This was to ensure that samples of all sizes were tested in AO exposure and the control environment, since the geometry of the samples affected the calculated short beam shear strength. There were some differences in sample top and bottom faces due to the curing process, so both were tested over the course of this research. In Fig. 5.2, the two faces are depicted. The left sample has the top side from curing and water jet cutting facing up, which resulted in a slight angle on the edges. The right sample has the flatter, bottom side facing up.

The face plate for three-dimensional samples was used in the MAX chamber. Since the intended sample troughs are holes, aluminum tape was used to create a surface to place the samples on, as shown in Fig. 5.3. This setup was chosen because it allowed for a variable number of samples to be tested at a time and could be used for other concurrent research. A rectangular Kapton witness

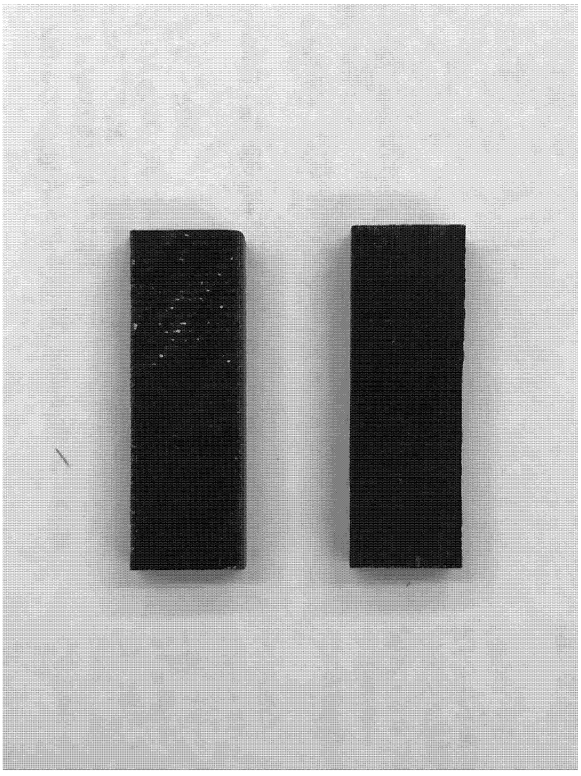

Figure 5.2: Sample Face Differences

sample was held between the two slots towards the edge of the face plate using aluminum tape flaps to hold it in place for Tests 2 through 7. For Test 1, the Kapton witness sample was simply placed on the tape surface with the samples near the center of the face plate. Figure 5.4 shows the Kapton witness sample and composite specimens inside the MAX chamber. Concurrent research characterizing the difference in AO fluence seen in different parts of the chamber showed that the AO fluence seen at the center of each trough was higher than that seen at the ends [19], as will be discussed in Section 7.1.

After the AO exposure was complete, the samples remained under vacuum in MAX until they were ready for mechanical testing, depending on the availability of the Structures and Composites Lab equipment. Control samples remained in Junior during this time period as well. All samples were removed from vacuum

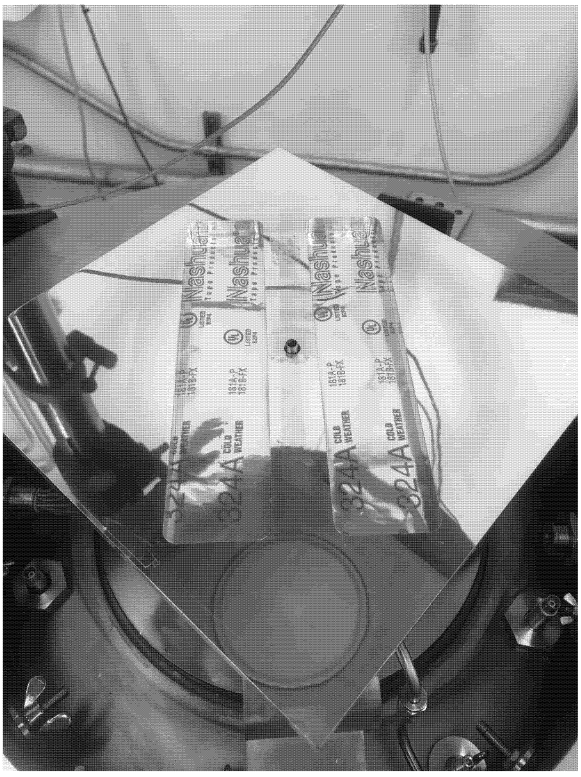

Figure 5.3: Aluminum Tape Surface in Two-Slot Plate

and weighed before mechanical testing. The Kapton witness samples were also weighed at this time in order to determine the effective AO fluence of the test. This process occurred within 5 minutes of removal from vacuum, to avoid the recovery of water vapor into the material. Samples after environmental testing are shown in Fig. 5.5, with the top row being control samples and the bottom row being AO-exposed samples.

5.2 Contamination Testing

Samples were tested for particulate contamination using a process similar to ASTM E1216, Standard Practice for Sampling for Particulate Contamination by Tape Lift [20]. Teflon tape donated by the NASA Jet Propulsion Laboratory was used in order to avoid unintentionally delaminating the carbon composite

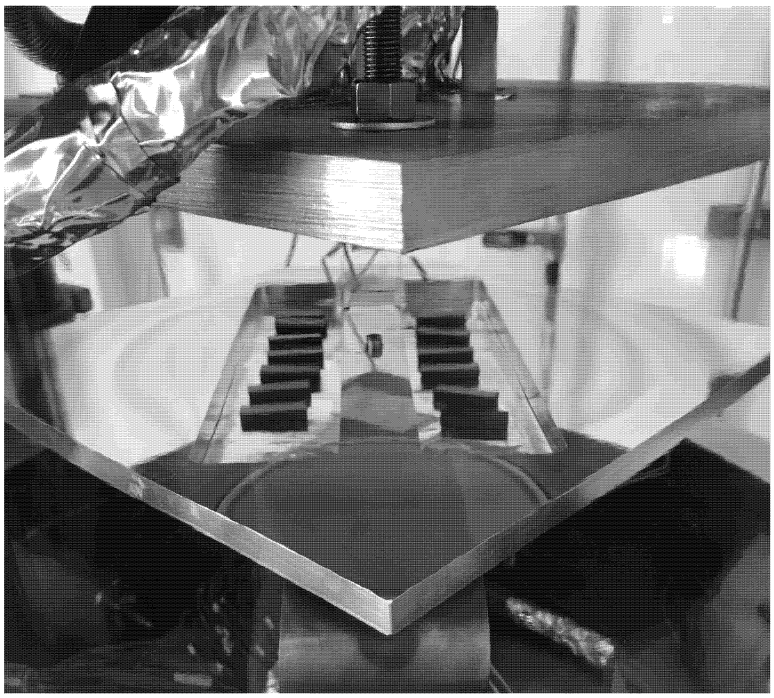

Figure 5.4: Samples within MAX Chamber

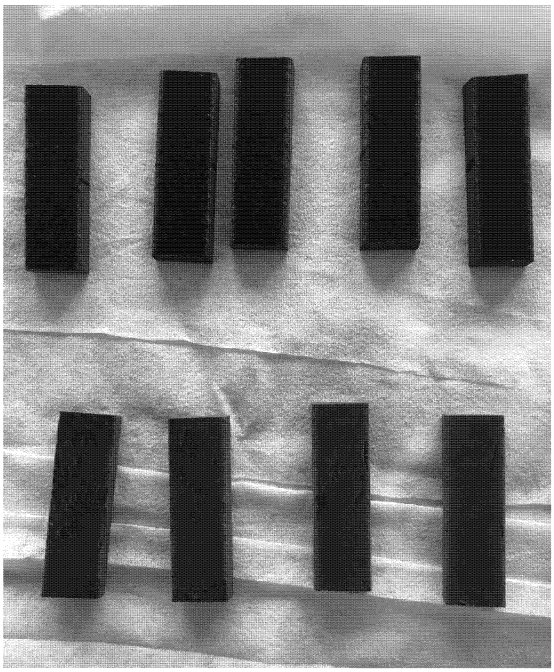

Figure 5.5: Samples after 48-Hour Exposure

samples. The tape lifts were taken in a generally clean environment, with all required elements being handled with gloves over a Kimtech wipe-covered surface. Tape lifts were only taken of the AO-exposure samples so that the cleanliness of each sample pre- and post-exposure could be directly compared.

Preliminary tape lifts were taken after the composite samples had been in bakeout for 48-hours and had been weighed. The samples were grossly cleaned with a KimTech wipe to reduce the initial particulate for the first tape lift. The tape was cut off of the roll, with one side that had been exposed during storage and the other that had not. Each tape lift was taken by placing the exposed side of the tape against a glass slide for support and pressing the unexposed side down onto the surface of the sample. The samples were then placed in MAX for AO exposure. The second set of tape lifts was taken after the samples were removed from MAX and weighed again. The tape lifts were stored between pre-cleaned glass slides until they were able to be imaged using a microscope, as discussed in Section 3.5.

5.3 Mechanical Testing

Samples were taken to the Structures and Composites Lab for mechanical testing on the Instron machine after weighing and contamination testing. Samples were tested in number order to reduce confusion between structural testing, mass, and size measurements. Each sample was tested once, with the same side facing up to the loading nose per test group. The samples could not be tested within 10 minutes of leaving the vacuum chamber due to contamination testing procedure beforehand and the limitations of the experimenter's efficiency. Therefore the samples were able to regain water vapor before mechanical testing occurred. The

Figure 5.6: Before and After Tape Lifts of Sample 36

samples were exposed to air for up to an hour in the cases of samples mechanically tested last. However, no trends were observed over each period of mechanical testing.

Testing was performed according to ASTM D2344, the Standard Test Method for Short-Beam Strength of Polymer Matrix Composite Materials and Their Laminates [18]. The required fixture had two support rollers placed 16mm apart with a single loading nose in the center, based on the sample geometry as described in Section 4.3. The crosshead movement was 1 mm/min, as prescribed in ASTM D2344. Each sample was tested to failure, defined as being a load drop-off of at least 30%. Each sample was placed onto the support rollers and centered over their length with equal overhang. The crosshead was lowered to be close to the

sample without pre-loading. A sample at the end of testing is shown in Fig. 5.7.

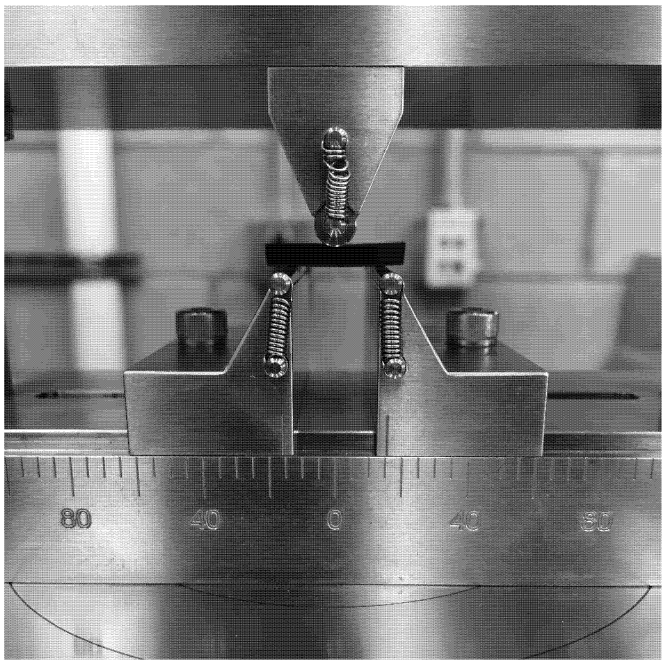

Figure 5.7: Specimen at Failure

Some issues in consistency were encountered during mechanical testing. There was some variation in the testing fixture setup between Test 1 and 2, Test 3, and Tests 4 through 7 as shown in Fig. 5.8. Test 1 and 2 were conducted using the standard setup, with the upper short beam shear fixture directly attached to the crosshead. However, the attachment screw for the crosshead fixture was found to be bent after Test 2. Therefore, Test 3 was performed slightly off-center which, combined with experimenter's error, created the differences in tests as discussed later in Section 7.3. The fixture was placed between two compression plates towards the front and secured with double-sided tape. After this, a modified centered setup was used for Tests 4 through 7, where the upper short beam shear fixture's crosshead attachment was taped to the upper compression plate.

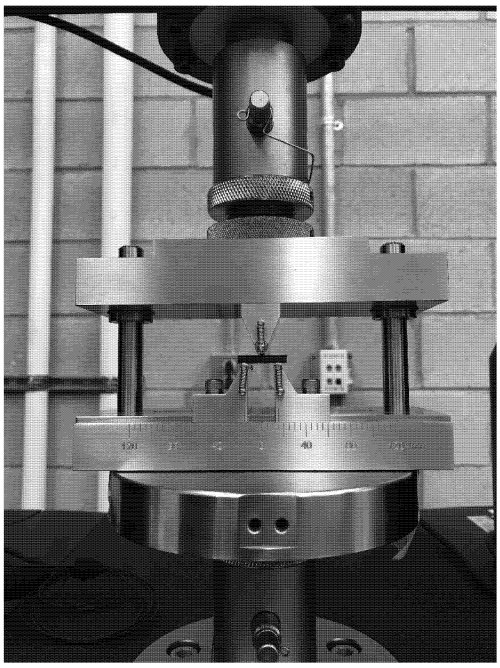

(a)

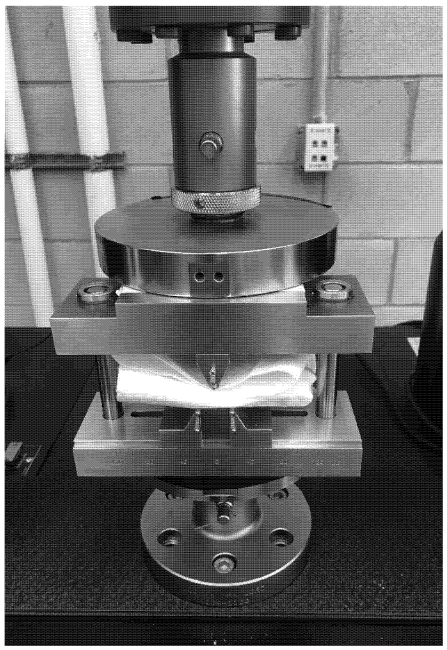

(b)

(c)

Figure 5.8: Short Beam Shear Setups for (a) Test 1-2 (b) Test 3 (c) Test 4-7

Chapter 6

ANALYSIS

This chapter explains the methods of analysis used to generate the results of this research. It explores the parameters of interest, the required statistical analysis, and error analysis. The last section discusses the sources of error for contamination analysis.

6.1 Parameters of Interest

An important measure of the AO exposure in a test is the effective atomic oxygen fluence, which is determined by the exposure area and mass loss of each Kapton witness sample in this research. This is used to estimate the AO exposure for the samples during each test, as well as for approximating the equivalent time on-orbit. Since Kapton HN is a standard witness material for ASTM E2089, its erosion yield on-orbit (3.00×10^{-24} cm^3/atom) has been determined empirically [10].

As given in the ASTM standard, the effective AO fluence seen by the witness sample can be calculated using equation 6.1 [10], with the variables of mass change Δm_k (g), exposed area A_k (cm^2), density ρ_k (g/cm^3), and erosion yield on-orbit E_k (cm^3/atom) for the witness sample. This results in a calculated effective AO fluence in atoms/cm^2.

$$F_k = \frac{\Delta m_k}{A_k \rho_k E_k} \tag{6.1}$$

Since the tested samples were small, the VeriTas precision balance could be

used to measure the change in mass of the samples in grams. The percent total mass loss (%TML) was calculated using equation 6.2 [10]. This is a measure of how much material has been eroded by the exposure to atomic oxygen. Since the composite is made of carbon fiber and epoxy, the %TML will encompass both epoxy molecules that have been eroded from interactions with AO and any carbon fibers that have been removed. This is also a significant factor that implies the production of contamination on-orbit. This non-dimensional value can be compared between treatments for both the 24-hour and 48-hour exposures using independent samples t-tests.

$$\%TML = 100 \times \frac{m_0 - m_f}{m_0} \tag{6.2}$$

In order to estimate the particulate contamination generated by the samples, the images taken of the tape lifts were analyzed for percent area coverage (PAC). This is a value that measures the percent of area in an image that is covered by particulate. In this research, the PAC was calculated using the number of dark pixels of particulate in the image against the light pixels of the tape. Since the tape lifts were taken before and after the AO-exposure, a paired-samples t-test was used to look for a difference. The null and alternative hypotheses for this analysis are shown in equation 6.3, where μ_d is that the mean difference between the PAC before and after treatment.

$$H_0 : \mu_d = 0; H_a : \mu_d < 0 \tag{6.3}$$

Finally, the short beam strength is used to compare the structural effects of AO on the composite samples. Shown in equation 6.4 [18], this parameter is calculated in MPa using the maximum load measured during mechanical testing

P_m (N), the sample width b (mm), and the sample thickness h (mm). The difference in short beam strength between treatments for 24-hour and 48-hour exposures can be calculated using an independent samples t-test, similar to the %TML comparison.

$$F_{SBS} = 0.75 \times \frac{P_m}{b \times h} \tag{6.4}$$

6.2 Statistical Analysis

When performing statistical analysis, the goal is to determine the statistical significance of the results. For a statistical test, there are two hypotheses: the null hypothesis, where there is no difference between the compared groups, and the alternative hypothesis, where there is a difference between the compared groups [21]. Statistical analyses use the p-value to quantify the risk that the null hypothesis will be rejected when it is actually true. A p-value of 0.05 is most typically used as a cutoff to determine if a difference qualifies as statistically significant [21].

In order to analyze the difference between multiple groups, one-way analysis of variance (ANOVA) was used [21]. This test determines if any differences exist between the testing groups of samples. If it is found that differences exist between groups, post hoc analysis must also be conducted. The Tukey post hoc analysis is used in conjunction with one-way ANOVA to determine which testing groups are different from each other [21]. The Tukey post hoc analysis calculates a p-value for each comparison. This post hoc analysis is valid when the variance within groups can be assumed to be equal. The combination of one-way ANOVA and Tukey post hoc analysis was used to determine differences between the testing

groups for %TML and short beam strength. If the differences between testing groups is large (p-value < 0.05), the test results should not be compared.

In statistical analysis, t-tests are used to compare means between two groups [21]. In order to compare the parameters of interest across the two treatments (AO-exposed and control), the independent samples t-test was used. This statistical analysis compares the parameters for each of the groups assuming that they have equal variance. The paired samples t-test was used to compare the PAC from before and after treatment. This statistical test is used because the parameters are not independent of each other.

6.3 Error Analysis

The error analysis for the AO fluence, %TML, and short beam strength can all be estimated using the uncertainty in a function of several variables, shown in equation 6.5 [22]. This calculation is straightforward with the use of differential calculus. The uncertainties within the equation are determined from either the established uncertainty of constants, or the repeatability or readability of measured variables. For variables measured multiple times, the repeatability was used as the uncertainty; for variables measured a single time, the readability was used. This equation is then capable of propagating these uncertainties forward into the final parameter of interest for AO fluence, %TML, and short beam strength [22].

$$\delta q = ((\frac{\partial q}{\partial x}\delta x)^2 + (\frac{\partial q}{\partial y}\delta y)^2 + ...)^{1/2} \tag{6.5}$$

The error for the mass difference for AO fluence in equation 6.6 and %TML in equation 6.7 was calculated using the repeatability of the VeriTas precision balance (0.0005 g). The error in measured area was approximated to be 10%

of the area calculated by image analysis software ImageJ. This error came from the limitations in area measured due to shadows and reflections on the Kapton film, similar to the errors in PAC discussed in Section 6.4. The error on the constants for density (0.01 g/cm^3) and erosion yield (1×10^{-26} cm^3/atom) were determined using the significant figures given. For the error in short beam shear strength in equation 6.8, the readability at the max load was used (0.001 N). The repeatability of caliper measurements was used for both the width and thickness measurements (0.005 mm).

$$\delta F_k = ((\frac{\delta \Delta m_k}{A_k \rho_k E_k})^2 + (-\frac{F_k \delta A_k}{A_k})^2 + (-\frac{F_k \delta \rho_k}{\rho_k})^2 + (-\frac{F_k \delta E_k}{E_k})^2)^{1/2} \tag{6.6}$$

$$\delta \%TML = ((\frac{100 m_f \delta m_0}{m_0^2})^2 + (-\frac{100 \delta m_f}{m_0})^2)^{1/2} \tag{6.7}$$

$$\delta F_{SBS} = ((\frac{0.75 \delta P_m}{bh})^2 + (-\frac{F_{SBS} \delta b}{b})^2 + (-\frac{F_{SBS} \delta h}{h})^2)^{1/2} \tag{6.8}$$

6.4 Sources of Error in Contamination Analysis

In the case of PAC, the error is less straightforward to analyze. Each tape lift was imaged in a grid of 3×10, resulting in 30 images per tape lift. However, if the tape lift was fully imaged, it would take approximately a 7×22 grid of images, resulting in 154 images per tape lift. This was not possible due to the time constraints and analysis requirements for the sheer number of images generated. Therefore, only approximately 20% per tape lift area was imaged using this grid pattern.

Overall, the PAC was underestimated due to some limitations of the hardware and software. In taking a picture, the microscope was only able to focus a limited amount; therefore, if the fibers attached to the tape were not flat, they would not be entirely in focus in the picture. In the imageJ software, these fibers would then become difficult to be counted since they contrasted less with the Teflon tape background, shown in Fig. 6.1. Additionally, the imageJ software could not count areas where the fibers were reflecting light and were therefore light colored, as in Fig. 6.2. Finally, due to their color, epoxy particulate was generally too light to be included in the PAC threshold for particle analysis, displayed in Fig. 6.3. However, these limitations are found when analyzing both the before and after images and are roughly equally present. Therefore, the results can be used as a low estimate of the generated particulate from the carbon fiber composites; the calculated results then can be used as a preliminary qualification for the material's use.

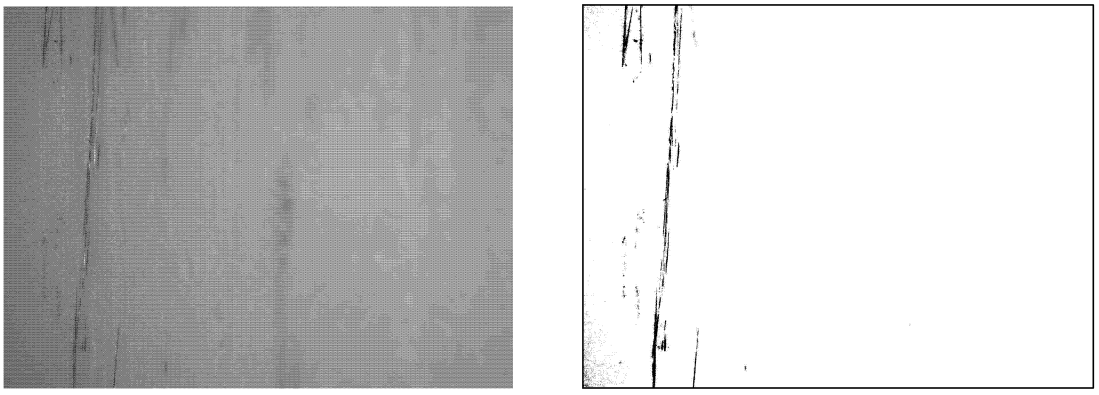

(a) (b)

Figure 6.1: Unfocused Image Example of PAC Error (Sample 87, After Middle) (a) Unfocused on Some Fibers (b) Resulting PAC Image

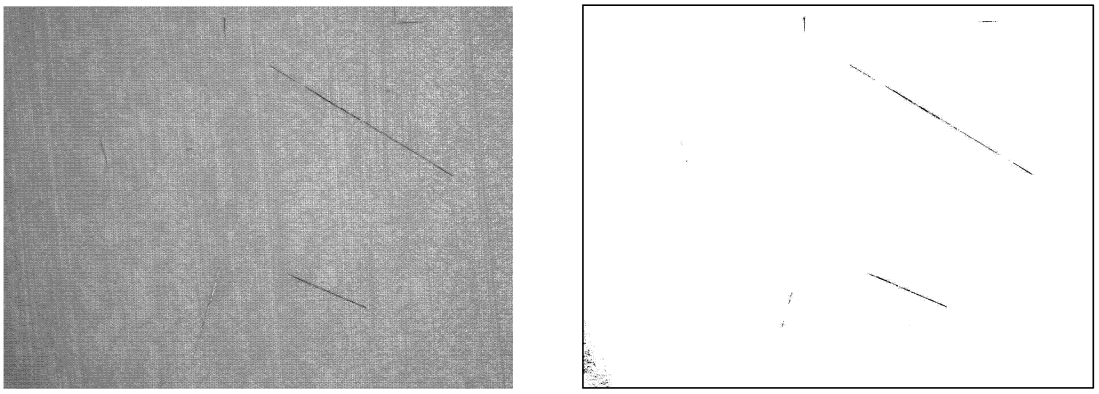

(a) (b)

Figure 6.2: Fiber Reflected Light Image Example of PAC Error (Sample 96, After Middle) (a) Reflective Fiber on Bottom Middle (b) Resulting PAC Image

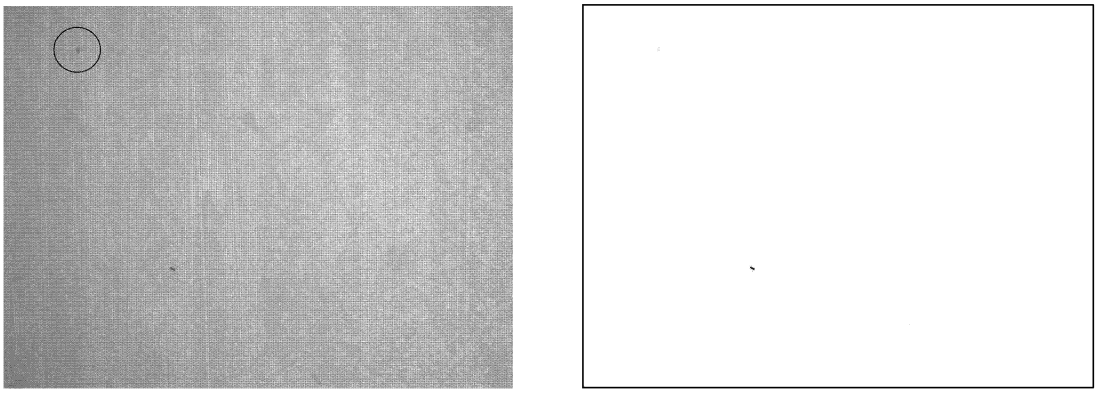

(a) (b)

Figure 6.3: Epoxy Particulate Example of PAC Error (Sample 99, Before Middle) (a) Epoxy in Top Left Corner (b) Resulting PAC Image

Chapter 7

RESULTS

This chapter will explore the results of this research. First, the exposure to atomic oxygen for all tests will be introduced. The effects on mass loss and contamination generation of the carbon composites will be discussed. Finally, the effects on short beam strength will be explored. Each section will also include the statistical analysis of the parameters of interest to determine if the AO-exposure create a significant difference from the control samples.

7.1 Atomic Oxygen Fluence

The equations 6.1 and 6.6 were used to compute the effective AO fluence and associated error for each test, which are displayed in Fig. 7.1. The mean AO fluence for the 24-hour tests was $(1.01 \pm 0.02) \times 10^{21}$ atoms/cm^2 and the mean AO fluence for the 48-hour tests was $(1.73 \pm 0.02) \times 10^{21}$ atoms/cm^2. This was calculated using the constants previously introduced in Section 6.1 for erosion yield and density and the mass loss and approximated exposed area. The mass loss was calculated as the difference of the averages of three readings from the precision balance before and after exposure. The area was calculated using the imageJ software. However, since the Kapton samples were not kept organized, an average exposed area from the imageJ calculations was used for the AO fluence and error calculations.

It can be seen that Test 1 had a higher AO fluence than the other 24-hour tests (Test 2-5). This is due to a difference in Kapton witness sample placement. Test 1 had the Kapton sample resting on the aluminum tape sample area. For

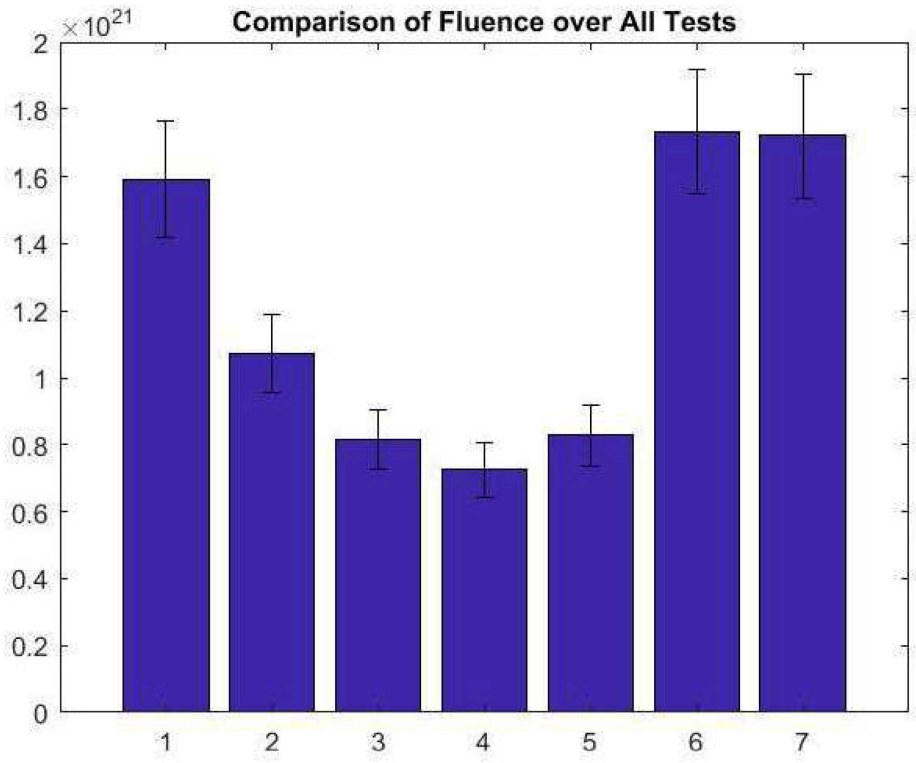

Figure 7.1: AO Fluence per Test

all other tests, an aluminum tape sleeve was created to hold the Kapton film against the plate at the end of the slot. Concurrent research showed a difference in the observed AO fluence across the face plate [19]. One test with only Kapton samples with the two slot face plate found that the AO fluence at the center of the plate was higher than the ends, with the results shown in Table 7.1. The test had locations 1-3 being placed in the left slot and 4-6 in the right slot [19]. This explains the difference in calculated effective AO fluence for the 24-hour tests due to witness sample placement. Additionally, the research found a standard deviation of the fluence of 0.1 $\times 10^{21}$ atoms/cm^2 over five 24-hour tests using the Kapton witness samples in the four-hole face plate [19]. The error in AO fluence calculated for each test is on a similar magnitude to this standard deviation.

Table 7.1: Two Slot Plate Calculated AO Fluence [19]

Location	Fluence (atoms/cm^2)
1	$9.67 \pm 0.09 \times 10^{20}$
2	$1.45 \pm 0.01 \times 10^{21}$
3	$8.08 \pm 0.06 \times 10^{20}$
4	$1.15 \pm 0.01 \times 10^{21}$
5	$1.33 \pm 0.01 \times 10^{21}$
6	$9.65 \pm 0.01 \times 10^{20}$

The importance of calculated effective AO fluence is the ability to estimate the correlating time on-orbit for a given orbit. A 400 km circular orbit with 28°inclination facing in with a surface in the RAM direction was chosen as an example case. This orbit is expected to see an atomic oxygen fluence of approximately 4.5×10^{22} atoms/cm^2 for a 15-year mission [7]. Assuming a linear relationship between fluence and time, the approximate time on-orbit was calculated. Utilizing the effective AO fluences seen in Tests 2-5, the approximate on-orbit time period was 12-18 weeks. For the two 48-hour tests, the approximate on-orbit time period was 29-30 weeks. However, these estimations are only valid for samples viewing similar AO fluence; from the concurrent research that was conducted, it can be assumed that samples at the center of the slot were exposed to a higher AO fluence than those at the ends of the slots [19]. For example, the AO fluence calculated from Test 1 has an on-orbit time of over 27 weeks. Therefore, the AO fluence seen by the samples is on the order of a few months at this orbit. Table 7.2 summarizes the results of the AO fluence calculations in this research, including sample location in the chamber, calculated AO fluence and error, and approximate time on-orbit for the given orbital case.

Table 7.2: Atomic Oxygen Fluence Results

Test	Duration	Sample Location	Fluence (atoms/cm^2)	On-Orbit Time
1	24-hr	Middle	$1.59 \pm 0.17 \times 10^{21}$	27.7 weeks
2	24-hr	End	$1.07 \pm 0.12 \times 10^{21}$	18.7 weeks
3	24-hr	End	$8.15 \pm 0.89 \times 10^{20}$	14.2 weeks
4	24-hr	End	$7.24 \pm 0.80 \times 10^{20}$	12.6 weeks
5	24-hr	End	$8.28 \pm 0.91 \times 10^{20}$	14.4 weeks
6	48-hr	End	$1.73 \pm 0.19 \times 10^{21}$	30.2 weeks
7	48-hr	End	$1.72 \pm 0.19 \times 10^{21}$	29.9 weeks

7.2 Mass Loss and Particulate Contamination

Samples from Tests 2 through 7 were measured for mass loss, resulting in 83 samples from 24-hour exposures and 57 samples from 48-hour exposures. Samples from Test 1 were not tested due to an oversight by the experimenter and control samples from Test 5 were not measured after they became disorganized from an experimenter's error while moving the desiccator's cart. The percent total mass loss (%TML) and associated error was calculated as described in equations 6.2 and 6.7 from Section 6.3. The descriptive statistics for the %TML are shown in Table 7.3.

Table 7.3: %TML Descriptive Statistics

	Mean	Std. Deviation	Mean Error	Minimum	Maximum
24hr AO-Exposed	1.503	0.6630	0.0646	-0.5857	4.513
24hr Control	-0.08846	0.2939	0.0642	-0.6018	0.8289
48hr AO-Exposed	3.133	0.4564	0.0664	2.075	3.740
48hr Control	0.06600	0.2217	0.0674	-0.3252	0.4791

The %TML for the 24-hour tests was first compared using a one-way ANOVA to ensure that there was not too large of variation between tests. It was found that there were no significant differences between tests for AO-exposed samples; for control samples, a significant difference between Test 2 and 4 (p-value = 0.002) and Test 2 and 5 (p-value = 0.000) was found. However, Test 2 had half

as many samples as Tests 4 and 5, making it a poor comparison, so the data was not removed. There was a statistically significant difference between the %TML of the AO-exposed and control samples (p-value = 0.000) with a mean difference of 1.592% and a standard error of 0.1137%. This was the expected result because it has been shown in previous research that AO erodes the exposed surface of carbon composites, reacting with the polymer epoxy [6].

For the 48-hour tests, no significant difference in %TML was found using an independent samples t-test across Tests 6 and 7 for AO-exposed (p-value = 0.266) or control (p-value = 0.378) samples, meaning the results could be compared across the two tests. Another independent samples t-test found a significant difference between the AO-exposed and control samples (p-value = 0.000). There was a mean difference of 3.067% with a standard error difference of 0.09558%. The AO-exposed samples lost more mass than the control samples in both the 24-hour and 48-hour cases; additionally, the %TML of the 48-hour AO-exposed samples was higher than the 24-hour AO-exposed samples. This result means that the AO reacted with the epoxy and either outgassed or physically removed particles from the material surface to create mass loss. Some fibers that were no longer attached to the material due to the eroded epoxy may have also been lost during sample handling and contributed to the %TML.

The %TML increased as the exposure time increased, as expected. The degradation of the surface of the samples is visible in the change from shiny to matte. The glossy finish to carbon composites is generally due to a surface layer of resin, while the matte finish on the AO-exposed samples is associated with exposed carbon fibers. The analysis of the particulate contamination generated due to AO exposure aimed to qualify the type of particulate created, determining if the top layer of resin had eroded to expose fibers or if the resin had only thinned.

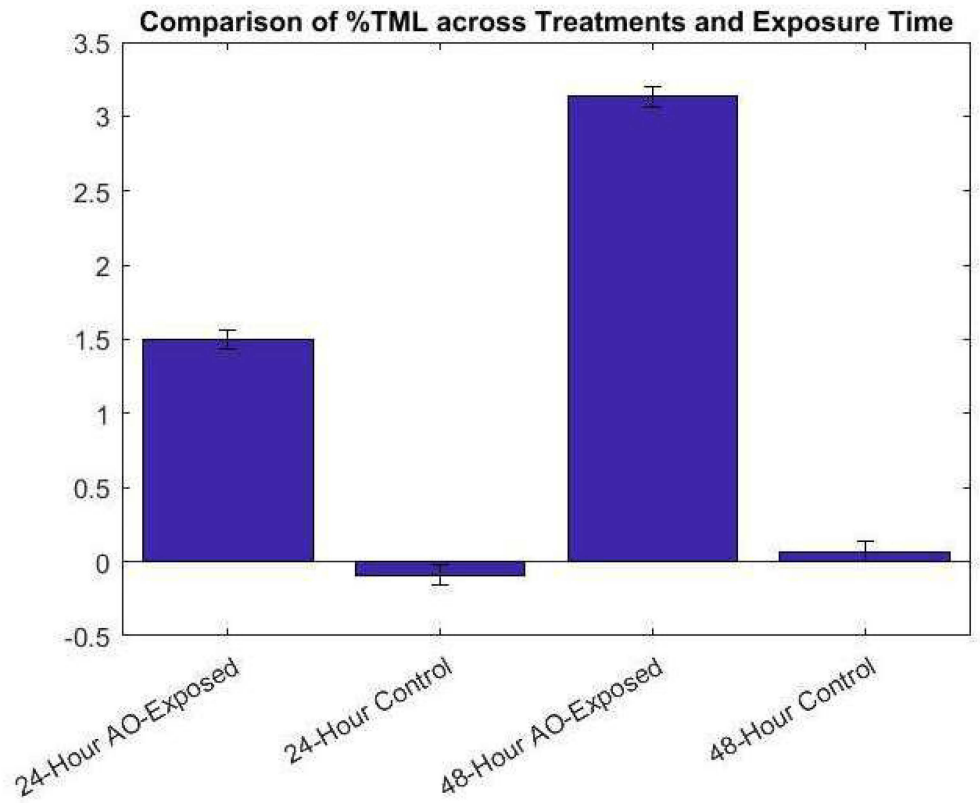

Figure 7.2: Mean Sample %TML per Treatment

Twenty samples tape lifts from the 24-hour exposure Test 4 and Test 5 were chosen for particulate contamination analysis. Twenty samples were chosen due to the time constraints of the experimenter given the 3×10 image grid per tape lift. These samples were chosen because the experimenter's skill in acquiring tape lifts increased over the experimental process; samples from the later tests were more uniformly applied tape lifts. Upon examination with 100x magnification on the optical microscope, it was seen that pre-exposure tape lifts had little to no particulate, with some very short carbon fibers. On post-exposure tape lifts, longer carbon fibers were found throughout, with larger concentrations on the ends. Across all samples, there was irregular particulate, likely from the environment and some outliers that included larger pieces of composite.

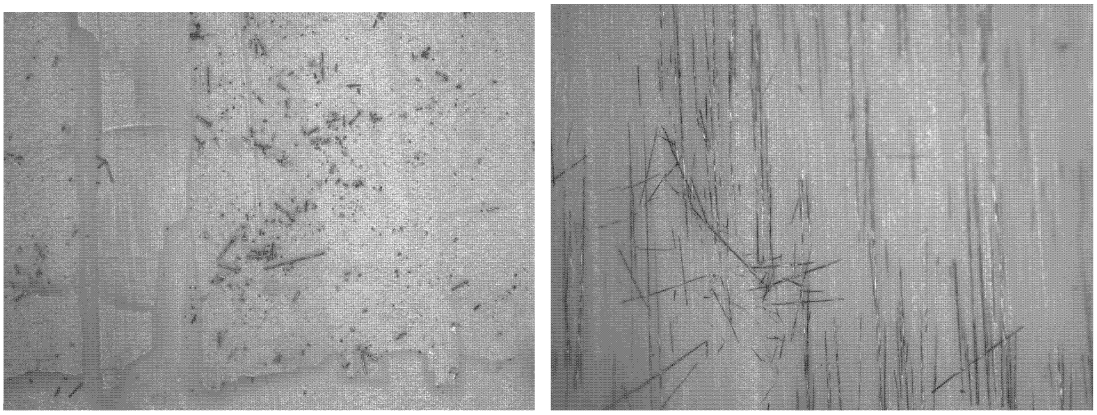

(a) (b)

Figure 7.3: Tape Lift Images from (a) Before Tape Lift, Sample 91 (End) and (b) After Tape Lift, Sample 91 (End)

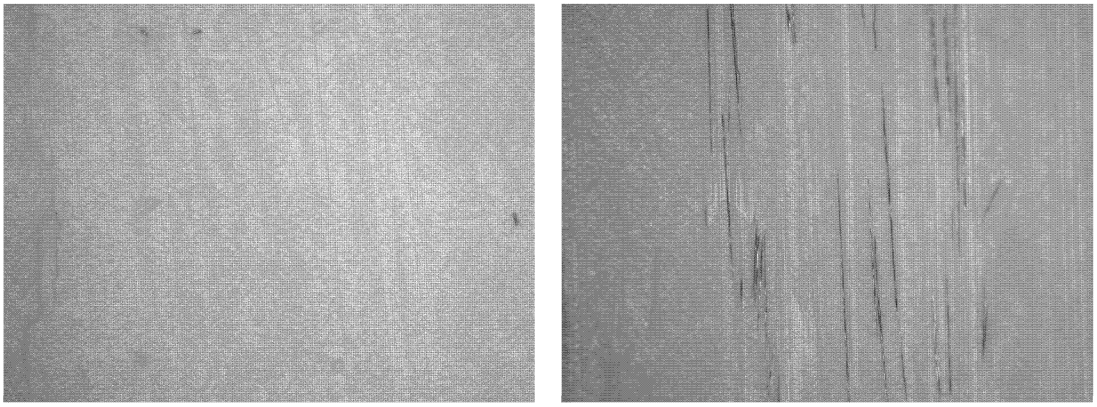

(a) (b)

Figure 7.4: Tape Lift Images from (a) Before Tape Lift, Sample 91 (Middle) and (b) After Tape Lift, Sample 91 (Middle)

It was found in an independent samples t-test that there was a significant difference between the particulate found on the ends of tape lifts and the middle of tape lifts (AO-exposed p-value = 0.000, control p-value = 0.000). Therefore, the pre- and post-exposure tape lifts will be separated by tape lift image location for comparison.

A paired samples t-test was used to compare the tape lifts taken before and after the AO exposure. For the images from the end of the sample, a significant

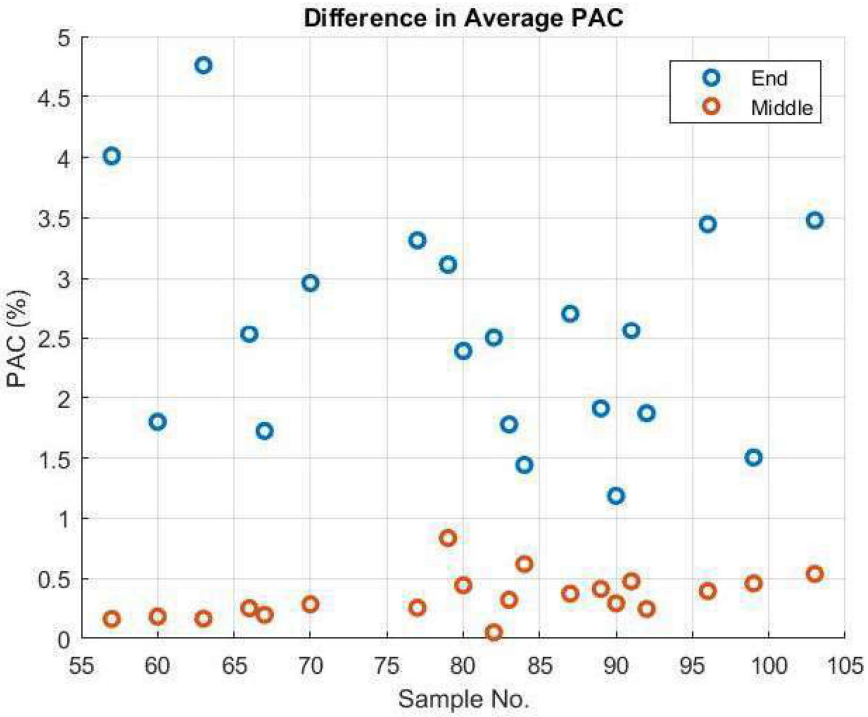

Figure 7.5: Difference in PAC per Sample

difference was found (p-value = 0.000), with a mean difference of 2.550% and a standard deviation of 0.9371%. For images from the middle of the sample, a significant difference in PAC was also found (p-value = 0.000) with a mean difference of 0.3478% and standard deviation of 0.1825%. For both the ends and middle of the composite samples, a noticeable increase in particulate was observed.

Table 7.4: PAC Descriptive Statistics

	Mean	Std. Deviation	Minimum	Maximum
Before PAC (End)	0.2441%	0.1697%	0.0632%	0.5610%
Before PAC (Middle)	0.0358%	0.0675%	0.0025%	0.2866%
After PAC (End)	2.7937%	0.9884%	1.4177%	5.1852%
After PAC (Middle)	0.3836%	0.1700%	0.1701%	0.8484%

Another way to describe the cleanliness of a surface in relation to particulate

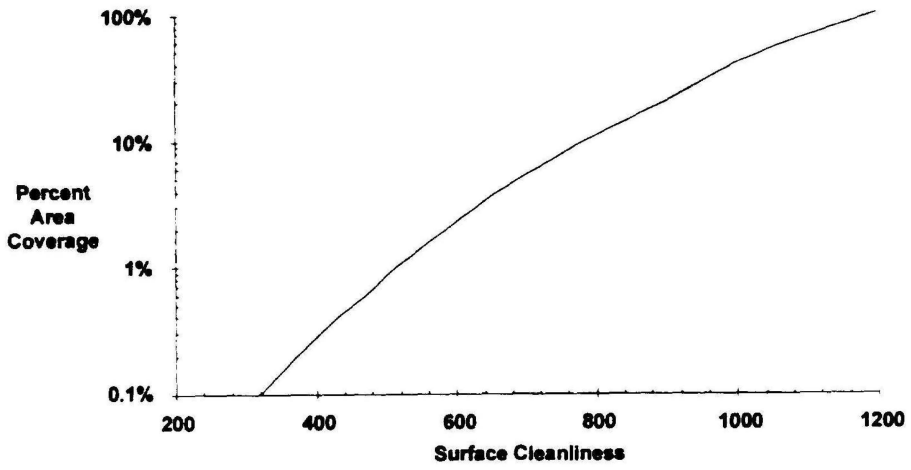

Figure 7.6: PAC and Surface Cleanliness Relationship [13]

contamination is particle cleanliness level (PCL). PCL is more accurate than PAC due to the incorporation of the size and number of particles within the examined area to the calculation. Typically, PAC is described as a function of PCL. Since the PCL was not measured explicitly in this research, it can be approximated from the calculated PAC. Figure 7.6 shows the relationship of PAC as a function of PCL, which was used to estimate the PCL for the given PAC. For the results found in this research, the average PCL pre-exposure was about 325 on the ends and less than 300 in the middle. The average PCL post-exposure was about 550 on the ends and 350 in the middle.

The higher calculated PAC post-exposure means that AO-exposure generates particulate contaminants from carbon fiber composites. The fibers become detached when the epoxy holding them in place is eroded away by the atomic oxygen. The delamination at the ends of the sample also increases the PAC, especially after the epoxy has been eroded. This result should be considered when materials are being selected for space applications like solar panel structures. If

exposed to AO, these structures will generate particulate contaminants and put the cleanliness of the spacecraft's sensitive components at risk. This data shows that a preliminary qualification for the use of this material near sensitive surfaces in an environment containing AO is necessary due to the risks of particulate contamination.

7.3 Short Beam Shear Strength

All samples produced were mechanically tested to failure for short beam shear strength, with 103 samples from 24-hour exposures and 52 samples from 48-hour exposures. One outlier from the 24-hour tests was omitted from analysis. This sample was observed to have a physical defect, and the resulting short beam strength was over 4 standard deviations from the mean. The short beam shear strength and its associated error were computed using equations 6.4 and 6.8 from Section 6.3. The calculated short beam strength for the AO-exposed and control samples are shown in Fig. 7.8 for 24-hour tests and Fig. 7.9 for 48-hour tests.

It can be seen in the 24-hour tests in Fig. 7.7 that there are three groupings: data from Tests 1 and 2, data from Test 3, and data from Tests 4 and 5. The data from Test 1 and 2 is scattered around the average, data from Test 3 is notably grouped below the average, and data from Tests 4 and 5 is above the average. Using a one-way ANOVA for each treatment, it was determined in the Tukey Post Hoc comparisons that there was a significant difference between Test 3 and all other tests. This was likely due to the different setup configuration from Test 3, as described in Section 5.3, causing an off-center application of force to the samples. Therefore, it was decided that the data from Test 3 would be eliminated from further analysis. In the one-way ANOVA, it was found that there were some

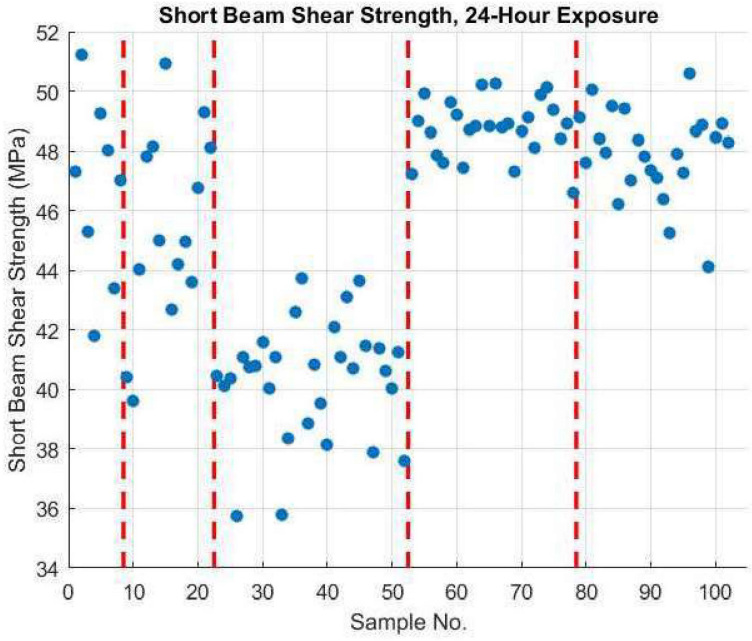

Figure 7.7: 24-Hour Short Beam Strength Divided by Test

differences between Tests 1 and 4, Tests 1 and 5, Tests 2 and 4, and Tests 2 and 5, but this data was included due to the small samples sizes from these tests making it a poor statistical comparison. These differences stemmed from the two different laminate sheets and learning curve of the experimenter. The p-values from this statistical analysis are shown in Table 7.5.

Table 7.5: One-Way ANOVA Tukey Post Hoc Results to Compare Tests

AO	1	2	3	4	5	Control	1	2	3	4	5
1	-	.735	.000	.039	.091	1	-	.907	.000	.865	.996
2	.735	-	.001	.000	.000	2	.907	-	.000	.148	.953
3	.000	.001	-	.000	.000	3	.000	.000	-	.000	.000
4	.039	.000	.000	-	.981	4	.865	.148	.000	-	.329
5	.091	.000	.000	.981	-	5	.996	.953	.000	.329	-

In an independent samples t-test, it was found that there was no significant difference between the two 48-hour tests (p-value = 0.359). Table 7.6 shows the descriptive statistics of the short beam strength for both the 24- and 48-hour

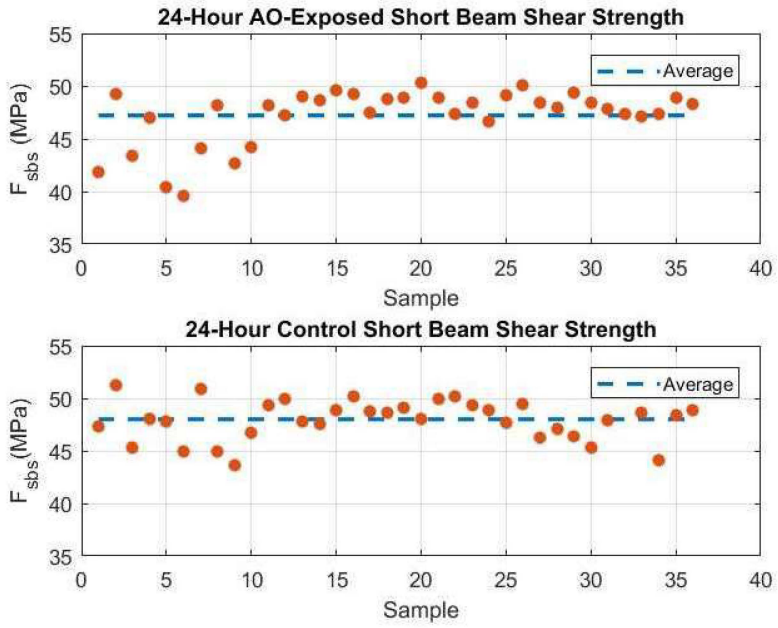

Figure 7.8: Calculated Short Beam Strength for 24-Hour Treatment with Reduced Data

exposed samples. For both types of tests, the mean short beam strength for the control samples was higher. However, there was greater standard deviation in the samples from the 24-hour tests than the 48-hour tests.

Table 7.6: Short Beam Strength Descriptive Statistics

	Mean	Std. Deviation	Mean Error	Minimum	Maximum
24-Hr AO	47.18	2.678	4.393e-5	39.61	50.24
24-Hr Control	48.00	1.932	4.402e-5	43.59	51.23
48-Hr AO	45.08	1.413	4.611e-5	41.20	47.00
48-Hr Control	47.01	1.468	4.615e-5	44.22	49.92

With the data reduced to insignificant variation across tests, an independent samples t-test could be used to compare the AO-exposed and control samples. For the 24-hour samples, no significant difference was found between the short beam strength of the AO-exposed versus the control samples (p-value = .141). This may be due to the differences between test setups and the two manufactured laminates. However, it is also possible that not enough of the composite was

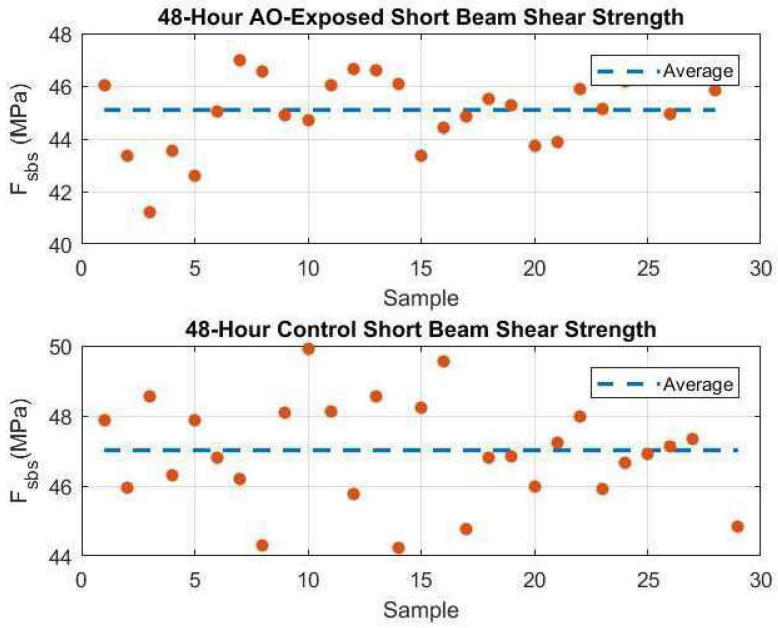

Figure 7.9: Calculated Short Beam Strength for 48-Hour Treatment

eroded in the AO exposure to create a significant difference between the two. The results of the tape lift showed that the epoxy had been eroded enough to detach carbon fibers. When looking at the calculated results for the 50 samples from Tests 4 and 5, the short beam strengths are tightly grouped. The samples are fabricated from the same laminate and the test setups are the same. This suggests that there is not enough epoxy eroded in the 24-hour exposure period to create a difference in the short beam strength.

However, a statistically significant difference was found between the AO-exposed and control samples for the 48-hour tests (p-value = 0.000). This analysis found a mean difference of -1.932 MPa and a standard error difference of 0.3819 MPa. As seen with the mass loss analysis, it is probable that enough of the composite was eroded by the AO exposure to meaningfully reduce the short beam strength. The results from the tape lift contamination analysis showed that the

epoxy had eroded to fully expose carbon fibers. This reduction in strength is due to the erosion of the epoxy and subsequent removal of the upper layer of carbon fibers. The measured difference is approximately 4% of the total short beam strength; depending on the space application of this material, this could be an acceptable degradation in strength over a component's lifetime.

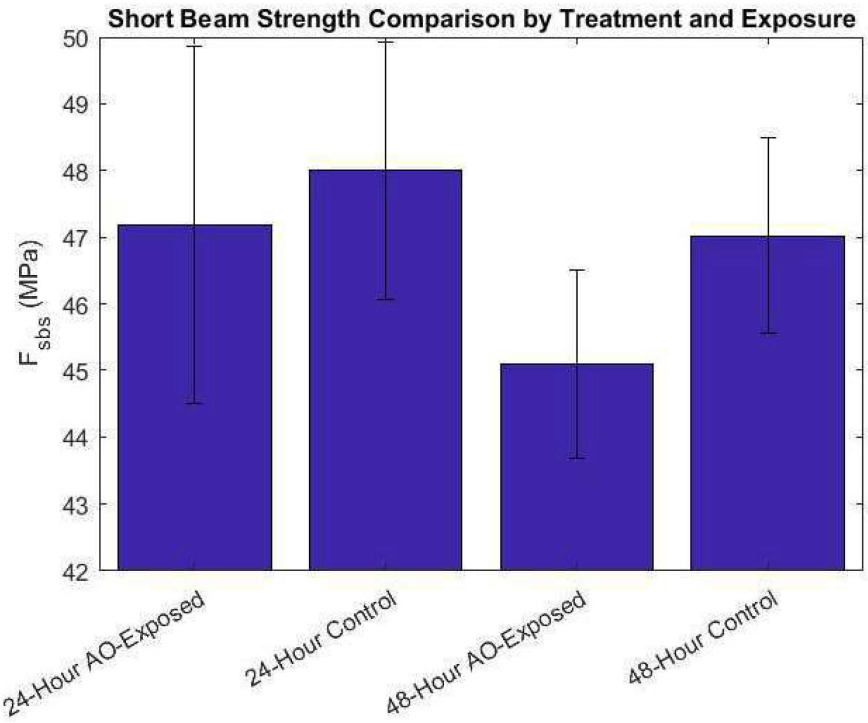

Figure 7.10: Comparison of Mean Short Beam Shear Strengths

Additionally, it was also observed that carbon fibers were coming off the top of the AO-exposed samples during mechanical testing. In Fig. 7.11, a slight fuzz of carbon fiber can be observed at the contact point between the fixture and the top surface of the sample. These fibers could be easily removed from the sample by brushing it, and the top roller of the fixture had to be cleaned of fibers after tests were completed. This is more evidence that the upper layer of carbon fiber has detached from the sample. This can be compared to the 24-hour sample

shown in Fig. 7.12, which shows the failure mode and AO degradation but no visible fibers above the surface.

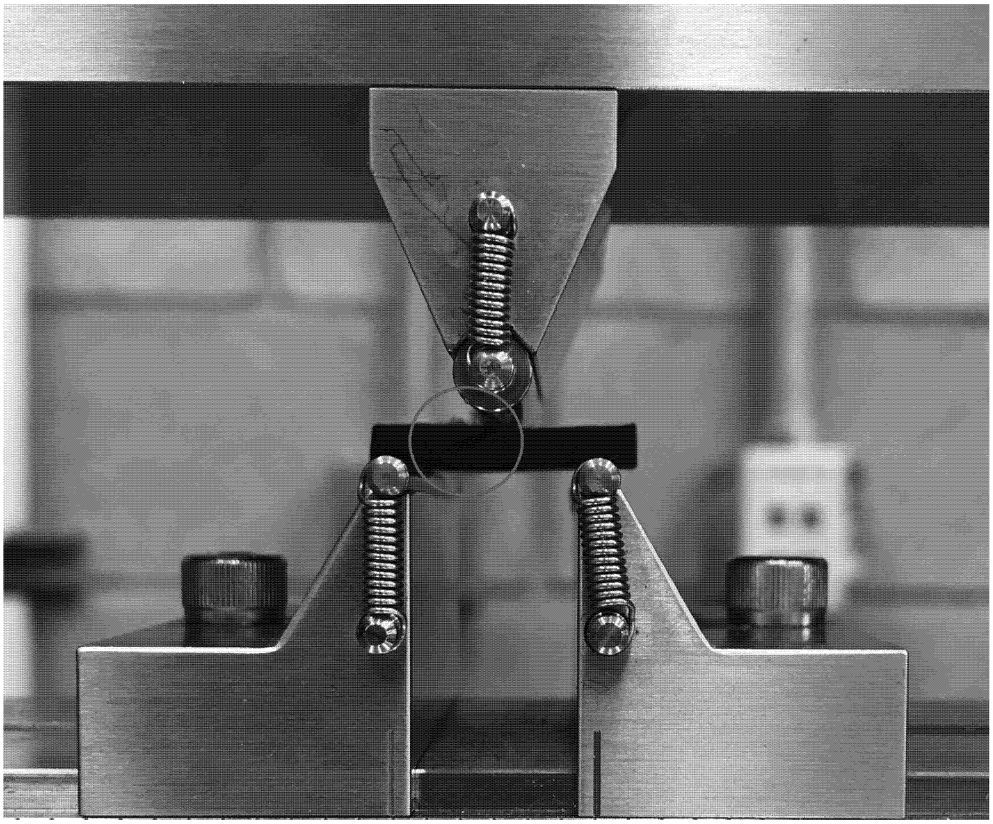

Figure 7.11: Carbon Fibers Visible at Mechanical Test Failure

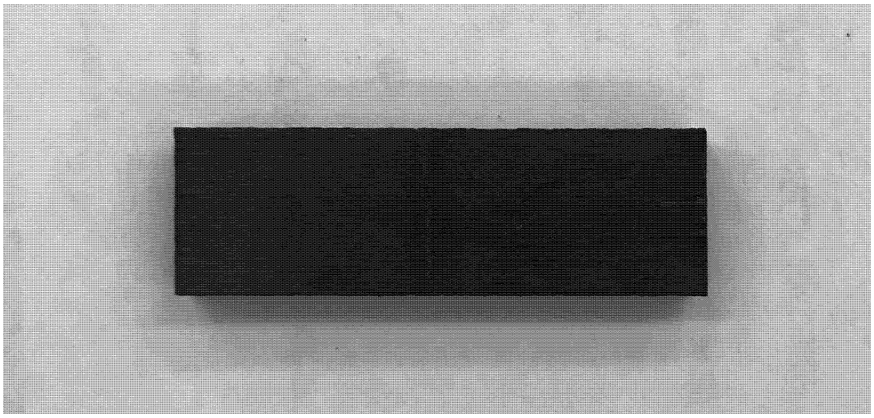

(a)

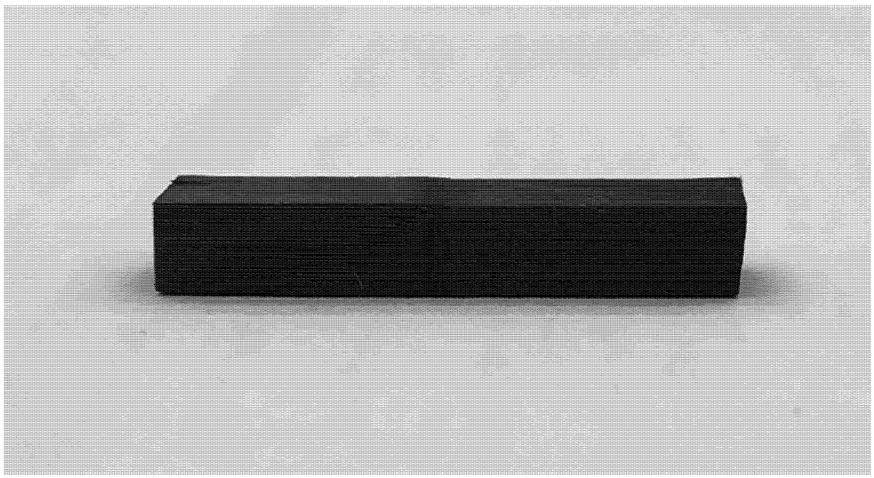

(b)

Figure 7.12: Samples after Mechanical Testing (a) Top View (b) Side View

Chapter 8

CONCLUSION

This chapter explores the results of this research in the context of space applications. The accomplished work and results will be summarized, followed by an examination of potential future work related to this research.

8.1 Atomic Oxygen Effects on Composite Samples

This research aimed to determine effects of atomic oxygen on the structural properties and contamination generation of carbon fiber composites. Previous research at Cal Poly SLO had found some correlation between AO exposure and the degradation of structural properties. It had also been observed that particulate contamination was generated from carbon fiber composites when exposed to atomic oxygen. This research tested the carbon fiber and epoxy composite samples for %TML, particulate contamination using tape lifts, and short beam strength.

The effects of AO on the material were measured using %TML and particulate contamination generation. As found in other research, exposure to AO increased the %TML of the samples when compared to the vacuum control samples. This average difference was 1.592 $\pm$ 0.1137% for 24-hour exposures and 3.067$\pm$ 0.09558% for 48-hour exposures. The particulate contamination was measured with the PAC of the tape lift images. It was found that images of the ends of the samples had higher PAC than images of the middles of the samples. When comparing the before and after images, the ends had a higher PAC by 2.550% and the middles had a higher PAC by 0.3478%. It was also observed that the

particulate was primarily long fragments of carbon fiber for post-exposure images and short fibers for pre-exposure images.

The work associated with contamination control for this research has implications for the use of carbon composites in space applications. With AO causing higher particulate generation, satellites using composites in the LEO environment should account for the higher quantity of carbon fiber particulate caused by interactions with atomic oxygen. If the particulate is disturbed from the surface, it can travel and contaminate a more sensitive surface on the spacecraft and negatively impact the spacecraft's performance.

The samples were also mechanically tested for short beam strength. No significant difference was observed between AO-exposed and control samples with 24-hour exposure periods. From the results of the tape lifts, the erosion of epoxy and release of a layer of carbon fiber was insufficient to cause a decrease in short beam strength. However, AO-exposed samples were shown to have a significant decrease in short beam strength compared to control samples for the 48-hour exposure period. This mean difference was 1.932 ± 0.3819 MPa, approximately 4% of the total calculated short beam strength. During mechanical testing, a fuzz of carbon fiber appeared above the exposed surface, suggesting that more fibers had been released due to epoxy erosion. Short beam strength is generally used as a measure of comparative testing [18], so there is not a direct application of these results to the use of this material. However, the data collected further characterizes the behavior of carbon composites in the space environment and can be used to predict their performance.

8.2 Future Work

The research performed in this thesis paves the way for future work conducted at Cal Poly SLO in space environments. The avenues of exploration for future research could be analysis of the environmental effects on composites exposed to AO, the contamination created by AO, or the change in material properties caused by atomic oxygen.

For work focusing on the environmental aspects for a three-dimensional sample, the addition of thermal cycling or UV radiation would be valuable. The thermal environment of MAX is not replicated in Junior, so some of the effects on structural properties may be due to these thermal differences. Previous research [12] shows that thermal cycling has large detrimental effects on carbon composites. However, these effects have not been entirely explored with the inclusion of AO in the environment. Additionally, the comparison of AO-exposed samples with thermally comparable control samples can isolate the effects of AO on the chosen material property. With the return of a deuterium lamp to MAX, the addition of UV radiation would increase the effects of atomic oxygen. Structural samples could then be tested in this synergistic environment to measure the amplification of previously seen effects. This research could isolate the effects of this exposure in addition to the AO environment.

For work focusing on the contamination aspects, research could expand on the quantification of the measured particulate. A similar tape lift test could be conducted, with analysis focusing not only on PAC but the size and number of particles on the tape lift. This would produce a more accurate PCL for the AO-exposed material. More qualitative analysis could be done by examining AO-exposed samples with an scanning electron microscope (SEM) to examine the

surface topography after AO-exposure. This could further pinpoint the extent that the epoxy is being eroded by the atomic oxygen. Alternatively, similar contamination analysis could be performed with samples having an AO-resistant coating (e.g. silicone). The addition of a coating to a material could be used to identify any reduction in generated contamination despite AO exposure.

For work focusing on the structural aspects, the limited use cases of AO-exposed structural components could be revisited. Another material parameter could be measured for a different mechanical testing setup, such as shear or impact testing. An expansion of Charles Ward's work with bending specimens with less variation in sample fabrication would also be applicable to the effects of thermal cycling on carbon composite solar panels. For a chosen environment including AO, a model could be developed to predict the response of a material. These results could be compared with experimental results and theoretical calculations. This could be applied to any chosen type of mechanical test, such as tension, shear, or short beam shear. Finally, mechanical fatigue testing could be used to compare AO-exposure to thermal fatigue. Samples could undergo AO-exposure and mechanical fatigue and be compared to thermally fatigued samples. The research could develop a relationship between mechanical and thermal fatigue, which AO could potentially affect similarly adversely.

REFERENCES

[1] Pisacane, V., *The Space Environment and its Effects on Space Systems,* AIAA Education Series, AIAA, New York, 2008.

[2] De Groh, K., Banks, B.A., Miller, S.K., "Low Earth Orbital Atomic Oxygen Interactions with Spacecraft Materials," NASA, Glenn Research Center, 2004.

[3] Ward, C., "Modification of a Ground Based Atomic Oxygen Simulation Apparatus to Accommodate Three Dimensional Specimens," California Polytechnic State University, San Luis Obispo, June 2018.

[4] Picone, J.M., Hedin, A.E., Prob, D.P., and Aikin, A.C., "NRLMSISE-00 Empirical Model of the Atmosphere: Statistical Comparisons and Scientific Issues," Journal of Geophysical Research, Dec. 2001.

[5] Glicklin, M.J., "Development of a Ground Based Atomic Oxygen and Vacuum Ultraviolet Radiation Simulation Apparatus," California Polytechnic State University, San Luis Obispo, June 2012.

[6] Han, J.H., Chun-Gon, K., "Low earth orbit space environment simulation and its effects on graphite/epoxy composites," Composite Structures, 2006.

[7] "Spacecraft Polymers Atomic Oxygen Durability Handbook," NASA, 2014.

[8] Banks, B.A., Waters, D.L., Thorson, S.D., Miller, S.K., deGroh, K.K., and Snyder, A., "Comparison of Atomic Oxygen Erosion Yields at Various Energy and Impact Angles," NASA TM-214363, 2006.

[9] Rutledge, S.K., and Banks, B.A., "Techniques for Synergistic Atomic Oxygen and Vacuum Ultra Violet Radiation Durability Evaluation of Materials for Use in LEO," NASA TM-107230, 1996.

[10] ASTM E2089-15, "Standard Practices for Ground Laboratory Atomic Oxygen Interaction Evaluation of Materials for Space Applications," ASTM International, 2015.

[11] Baluch, A.H., Park, Y., Kim, C.G., "Hypervelocity impact on carbon/epoxy composites in low Earth orbit environment," Composite Structures, 2013.

[12] Park, S.Y., Choi, H.S., Choi, W.J., Kwon, H., "Effect of vacuum thermal cyclic exposures on unidirectional carbon fiber/epoxy composites for low earth orbit space applications," Composites: Part B, 2012.

[13] Tribble, A.C., Boyadjian, B., Davis, J., Haffner, J., McCullough E., "Contamination Control Engineering Design Guidelines for the Aerospace Community," NASA, Marshall Space Flight Center, 1996.

[14] Chen, P.T., "Contamination Effects due to Space Environmental Interactions," NASA, Goddard Space Flight Center, 2001.

[15] VeriTas. "Top Loading "S" series MARK Balances," 2009.

[16] Toray Advanced Composites, "Solar Arrays for Next Generation Satellites," online.

[17] Tencate Advanced Composites, "RS-36 Resin System Product Data Sheet," 2018.

[18] ASTM D2344-16, "Standard Test Method for Short-Beam Strength of Polymer Matrix Composite Materials and Their Laminates," ASTM International, 2016.

[19] Glicklin, M., Abercromby, K., Ward, C., Reid, B., Griffith, C., "Atomic Oxygen and Vacuum Ultraviolet Radiation Simulation Chamber at California Polytechnic State University, San Luis Obispo," Applied Space Environments Conference, May 2019.

[20] ASTM E1216-11, "Standard Practice for Sampling for Particulate Contamination by Tape Lift," ASTM International, 2011.

[21] Salkind, N.J., Statistics for People Who (Think They) Hate Statistics, Sage Publications, 2016.

[22] Taylor, J.R., Introduction to Error Analysis: The Study of Uncertainties in Physical Measurements, 2nd ed., University Science Books, 1997.

Appendix A

OPERATING INSTRUCTIONS - JUNIOR

A.1 Prior to Operation

1. Ensure that the O-ring is sufficiently greased.
2. Secure samples inside the bowl.
3. Place the lid over the bowl.

A.2 Pumping Down

1. Rest the vent plug and vacuum retention valve assembly over the hole in the lid.
2. Ensure that both the ball valve and venting plug are closed.
3. Turn the pump to the "on" position.
4. Open the ball valve.

A.3 Bringing the Pressure Back to Atmospheric

1. Close the ball valve.
2. Turn the pump to the "off" position.
3. Twist and pull up on the vent plug until you start to hear the air entering the chamber. Avoid this getting too loud as venting too quickly can dry out parts of the chamber and cause cracking.

4. Once the pressure inside is in equilibrium with the atmosphere, the lid should lift off the bowl easily. It is sometimes preferred to move the desiccator with the lid on. In this case, the vent plug and vacuum rentention valve assembly can be lifted off.

Appendix B

OPERATING INSTRUCTIONS - MAX

B.1 Safety Concerns

1. The intent of this section is not to address all the safety concerns encountered in the Space Environments Lab at Cal Poly SLO. It is the user's responsibility to ensure that all lab safety procedures are adhered to.

2. As with any space environments chamber, do not operate without first receiving proper training in safety and operation of this specific chamber.

    - Do not operate this apparatus alone. Those accompanying you must be instructed in how to shut down the system in the case that an accident occurs and you are unable to communicate.
    - You or someone working with you must also have Dr. Abercromby's direct number in case of urgent issues.

3. There is a bag of un-popped popcorn kernels mounted next to the radio frequency power source. The purpose of which is that in the unlikely event that potentially harmful amounts of energy are exiting the system, the popping kernels would serve as an indicator. If you smell, see, or hear the kernels popping, evacuate the lab and call Dr. Abercromby.

4. The system heats up to 93°C during a 24-hour test. Heated elements include but are not limited to the coaxial cable, DSS, and the base assembly. It is recommended that users let the system cool under vacuum before removing samples for weighing. Another option would be to wear protective gloves

when detaching the coaxial cable and removing samples.

B.2 Sample Preparation

1. Wear nitrile gloves to protect samples from contaminants on your hands. Fingerprints add weight.

2. Cut at least one Kapton HN witness sample, whose size is dependent on the base plate being used. The four-hole plate (FHP) will accept up to four 5 cm $\times$ 5 cm squares placed inside the four pockets. Plates like the two-slot plate that don't have an opening for defining the exposure area will require dimensions dependent on where the witness samples will be masked. If placing the witness sample(s) near the center of the two-slot plate, the Kapton should be cut to 3 cm $\times$ 2 cm unless otherwise desired.

3. Thin samples for studies on mass loss can be cut similarly to the witness sample(s) for the FHP. Structural elements should be prepared according to the standard(s) used in the study of interest and best practices depending on the material and what is available. Masking should be performed with aluminum tape around all surfaces except for those normal to the top electrode for which exposure is intended. This is due to the omnidirectional nature of the atomic oxygen. Surfaces may be omitted from this process if it is known that erosion will not occur due to the surface's position and orientation.

4. Per ASTM E2089, samples (witness or otherwise) should be placed in a vacuum under 200 mTorr for 48 hours or longer as required until mass loss due to moisture evaporation is not measured.

B.3 AO Exposure

1. Ensure that all vacuum control panel toggles are switched to the "off" position.

2. Ensure that the main three-phase, 3Φ, power cable from the back of MAX is plugged into a 2083Φ VAC breaker and rotated about 45 degrees clockwise.

3. Ensure that the 2083Φ VAC breaker is flipped to the "on" poisition. If it is not, announce to the lab that you are turnning on the 3Φ since it makes an alarmingly loud sound when toggled.

4. Ensure that the ball valve to the pressurized air line on the back of MAX is in the open position. There should be a pressure reading on the dial gauge in the back.

5. Flip the Main Power switch on the front control panel to the "on" position.

6. Turn on the Granville-Phillips 316 Vacuum Gauge Controller. Convectron gauge 2 indicates the pressure of the roughing line in Torr, and gauge 3 indicates the chamber pressure in Torr.

7. Prior to raising the hoist, ensure that the coaxial cable is not attached to the top of the chamber.

8. Use the hoist switch to raise the lid. **Note** that the hydraulic mechanism lags behind the switch. This poses a threat to the grounding wires that are fixed to the lid, as they will break off if the hoist is raised too far. The hoist switch must be released in anticipation of this.

9. Lift the side lever that pushes against the bell jar and remove the glass.

10. Remove samples from vacuum. At this point, the 5-minute period has started.

11. Weigh the samples (witness or otherwise) and place them in the chamber.

    - For exposing thin samples in the four hole plate:

      (a) **Note** that prior to removing thin samples from vacuum, it would be beneficial to practice this process to improve user efficiency. The following are specific instructions on how to secure the specimens, but different steps can be used depending on user preference and ability.

      (b) Place samples in the center of the four backing pieces.

      (c) Place two backings, one at a time, inside adjacent pockets. Make sure that the sample does not move around so much that the exposure area intersects the edge of the material.

      (d) Hold these in place with one hand. With the other, secure them by screwing in a thumb screw and washer between the two pockets. Once the thumb screw is secured, the two backings may be released.

      (e) Place another backing inside one of the two remaining pockets and secure it by screwing in another thumb screw and washer between this backing and the already installed adjacent backing.

      (f) Repeat the above for the remaining backing piece.

      (g) Secure the last thumb screw and washer.

      (h) Ensure that all samples are secured flush against the underside of each pocket and that each backing isn't tilted.

- For exposing thicker samples in the two slot plate or future plate designs:
  (a) If using a shim casing to hold samples, fashion this out of an acceptable chamber material such as stainless steel. An alternative to making shim casings is to use aluminum tape to secure samples underneath the slots.
  (b) The shim casing does not need to have overhang overlapping the top of the plate. Rather, it is recommended that the shim casing be taped to the interior of the slot, reducing damage to the top surface of the plate. Aluminum tape should be sufficient to hold casings and samples in place.
  (c) Place the sample inside the shim casing.
  (d) Mask the witness sample.
    - **Note** that as much of the following should be done in advance of removing samples from vacuum.
    - Cut four pieces of aluminum tape slightly longer than the four sides of the witness sample, and wide enough to be easily handled.
    - Carefully fold the tape on itself along its length to create a straight flap that has adhesive on neither side. The flap should be narrow since large ones are less likely to maintain contact with the witness sample.
    - After repeating the above process with all four pieces, place three of them on the surface of the plate to form three sides of a square with appropriate dimensions so that the witness sample will slide underneath all three flaps.

- Place the final piece of tape to secure the witness sample.
- Flatten all flaps to ensure good contact with the witness sample.

12. Once samples are loaded, replace the glass bell jar.
13. Lower the side lever that pushes against the bell jar.
14. Lower the lid using the hoist switch.
15. Attach the coaxial cable to the lid.
16. Ensure that all ports are closed, including the black nupro valve on the gas insertion line, the vent valve, and the valve to the roughing line.
17. Flip the Mechanical Pump Power and the Mechanical Pump switches to the "on" position.
18. On the mechanical pump control box, flip the switch to the "on" position.
19. Flip the Chamber Rough Valve switch to the "on" position.
20. Monitor the roughing line and chamber pressures. Without inducing a leak, the system should pump down to the order of 10s of mTorr.
21. The pump requires some time to warm up before stable equilibrium is possible. Allow the pump to run for 30 minutes.
22. Open the valve to the gas insertion line and adjust it to obtain an equilibrium pressure of 175 ± 10 mTorr. Monitor the chamber for several minutes to ensure stability.
23. Turn on the R301 generator.

24. Set the power to 125 W.

25. Turn on the MC2 controller.

26. Switch to manual adjustment mode and adjust the load and tune capacitors each to 50%.

27. Switch the adjustment mode back to auto for both tune and load. This is necessary or else the controller will not be able to reduce the reflected power.

28. Perform one last check for the chamber pressure. It should be steady at 175 $\pm$ 10 mTorr.

29. Turn on the RF power on the R301.

30. At this time, the MC2 will auto-adjust to find a stable point where the reflected power (REF) is 1 W or 0 W. If at any times the REF is greater than 0 W, manually adjust the tune and/or load until the REF is 0 W. If it is not possible to obtain 0 W REF, turn off the system and refer to the MC2 manual.

31. Adjust the phase and magnitude to be 0 $\pm$ 25 mV each. These can be adjusted by turning the potentiometers on the left-hand side of the AT3 unit.

32. Maintain the system at these settings for 24 hours, or the desired exposure period.

33. Turn off the RF power using the button on the R301 box.

34. Turn off the MC2 controller.

35. Turn off the R301 gnerator.

36. **Note** that the system is at an elevated temperature. Either wait for the system to cool or use protective gloves.

37. Disconnect the coaxial cable from the feedthrough port on the lid.

38. Close the valve to the gas insertion line.

39. Close the Chamber Rough Valve.

40. Flip the Mechanical Pump Power and Mechanical Pump switches to the "off" position.

41. Flip the Vent switch to the "on" position and fully open the valve to the gas insertion line. **Make sure** to flip the Vent switch to the "off" position when the chamber pressure reaches 700 Torr. Otherwise, the compressed air line will cause the lid to suddenly lift off of the chamber with a "pop."

42. Continue to vent the chamber through the gas insertion line.

43. Once the chamber pressure has reached equilibrium, use the hoist switch to raise the lid. While doing so, hold the coaxial cable out of the way in order to reduce strain on it. As before, **ensure** that the grounding cables are not strained by lifting the lid too high.

44. Remove the glass to gain access to the samples.

45. Remove the samples from the chamber to weigh them.

    - Using the four hole plate:

        (a) Remove one of the thumb screws and washers.

(b) While holding onto one of the backings adjacent to where the screw was removed from, remove its other adjacent thumb screw and washer. The backing will then come away from the pocket.

(c) Repeat this process with one of the backings adjacent to the previous.

(d) For the last two, first support both backings with one hand on each.

- Using the two slot or similar plate:

  (a) Remove whatever specimens were tested.

  (b) Remove one side of the witness sample masking.

  (c) Slide the sample out from under the remaining three flaps, making sure that the sample doesn't come in contact with any adhesive from the aluminum tape. If this is done carefully enough, three of the four aluminum pieces may be reused.

46. Weigh each sample (witness or otherwise) within 5 minutes from when the vacuum was lost.

47. Lower the lid when not in use.

B.4 Base Plate Replacement Procedure

1. Follow the instructions in section B.3 to open the chamber and remove the glass.

2. Prior to removing the plate currently installed, measure the height of the top surface of the base plate with respect to an easily reachable reference,

such as the top surface of one of the support bars below the plate. The positioning of the height of the replacement plate will need to be the same.

3. Loosen a nut on each of the threaded support rods underneath the base plate.

4. With some freedom from the rods, they can be unscrewed from the underside of the base plate.

5. Using an allen key, unscrew the two #10 screws that attach the grounding strap to the underside of the base plate.

6. The plate should now be easily removed.

7. Place the new plate over the support rods, lining up the center hole with the opening of the insertion line.

8. Screw the support rods into the underside of the plate as well as the #10 screws that hold the grounding strap to it.

9. Place a level on top of the plate. Adjust the nuts on each support rod so that the top surface is the same distance from the reference as the previous plate and that the plate is level.

10. Once the plate is installed, continue with the steps in Section B.3 to test that the setup can be stabilized.

Appendix C

OPERATING INSTRUCTIONS - INSTRON

C.1 Safety Concerns

1. The intent of this section is not to address all the safety concerns encountered in the Aerospace Engineering Structures and Composites Lab at Cal Poly SLO. It is the user's responsibility to ensure that all lab safety procedures are adhered to.

2. As with any testing apparatus, do not operate without first receiving proper training in safety and operation of this machine.

    - Do not operate this apparatus alone. Those accompanying you must be instructed in how to operate the system in the case that an accident occurs and you are unable to communicate.

    - Additionally, all activities in the lab require prior risk assessment paperwork to be completed in advance.

3. Never place digits or limbs between loading and support noses.

4. All persons in the lab must wear proper safety equipment while testing is being performed.

C.2 Short Beam Shear Testing

1. Turn on the tower and accompanying desktop machine.

2. Log in to the Bluehill application. The manual controls for the tower will then be enabled.

3. Move the crosshead up until there is sufficient space to install and adjust the fixtures.

4. Set a compression support on the base fixture.

5. Install the compression support and tighten.

6. Set the load span on the base fixture.

7. Install the top fixture but do not tighten.

8. Place tape on the bottom of the base fixture and align the columns with the holes in the top fixture.

9. Lower the crosshead so that the base fixture is placed on the compression support.

10. Ensure that the columns are all aligned properly and tighten the top fixture.

11. Raise or lower the crosshead to allow a sample to be loaded.

12. Load sample on the support rollers. It should be centered on the length of the rollers and across the span.

13. On the computer, select the desired testing method.

14. Lower the crosshead so it is near the sample but no pre-loading occurs.

15. If desired, zero the extension and balance the load. **Note** that it is recommended to set the zero extension above the sample so that return commands will lift the crosshead above the sample.

16. Click “Start” to begin the test.

17. The Instron will then run the selected testing method. However, the test may be stopped at any time by clicking “Stop.”

18. If testing more samples, move the crosshead back above the sample. You can do this manually or by clicking “Return” if you set the zero extension above the sample.

19. Replace the sample with a new one and repeat the process of lowering the crosshead again until it is near the sample and clicking “Start” to run the tests.

20. Once finished testing samples, click “Save As” to choose a file name and location.

21. Click “Finish.”

22. Navigate to the chosen location and transfer the output data to a flash drive or other device for use later.

23. Move the crosshead up until there is sufficient space to uninstall the fixtures.

24. Remove the top fixture.

25. Remove the base fixture.

26. Remove the compression support.

27. Log out the Bluehill software, shut the computer down, and turn off the tower.

Appendix D

OPERATING INSTRUCTIONS - AUTOCLAVE

D.1 Safety Concerns

1. The intent of this section is not to address all the safety concerns encountered in the Aerospace Engineering Structures and Composites Lab at Cal Poly SLO. It is the user's responsibility to ensure that all lab safety procedures are adhered to.

2. As with any testing apparatus, do not operate without first receiving proper training in safety and operation of this machine.

    - Do not operate this apparatus alone. Those accompanying you must be instructed in how to operate the system in the case that an accident occurs and you are unable to communicate.
    - Additionally, all activities in the lab require prior risk assessment paperwork to be completed in advance.

3. Never attempt to open the autoclave door while it is under pressure.

4. When unlocking and opening the autoclave door, stand to the side of it rather than in front of it.

5. Check the air temperature before opening the autoclave. The system should be allowed to cool prior to retrieval of the part.

6. When removing objects from the autoclave, they can often be hotter than the air temperature reading. Use thick mittens to remove parts that could

still be at elevated temperatures. Place these on a surface unaffected by heat. Note that cutting surfaces in the lab are warped by heat.

D.2 Curing Procedure

1. Parts going into the autoclave should already be bagged and ready for cure.

2. Turn the autoclave power on by turning the large lever on the control box on the left side of the autoclave. Note that sometimes a meaningless alarm will sound as the autoclave control program loads. This can be silenced using a large red buttton on the control box labeled "Silence Alarm."

3. View the perimeter of the door. It has teeth along the outside. If these are offset from the teeth on the door lock, then the door is open. If they are lined up, then it is locked. If locked, turn on the hydraulics on the right side of the autoclave by turning the rotary switch, then toggle the lever to rotate the lock. If you do not hear the hydraulics turn on, then the safety lever is likely engaged and must be released. If you hear a screech almost immediately, toggle the lever the other way until you hear another screech. Turn off the hydraulics once the door is unlocked. If it's already unlocked, then continue to the next step.

4. Connect a vacuum pump to the vacuum supply line to the autoclave and turn it on.

5. Attach a hose between the port to the vacuum bag and the vacuum feedthrough port inside the autoclave.

6. Set the part down and check the bag for leaks.

7. Shut the door.
8. Turn the rotary switch to activate the hydraulics for the door lock.
9. Toggle the lever to secure the lock.
10. Turn off the hydraulics and engage the safety lever.
11. Sign in to the autoclave controller software.
12. You may select a recipe which will automatically follow a prescribed cure cycle.
13. You may also control temperature and pressure manually. **Note** that the fan should always be running while the autoclave is still in use. Also note that sometimes it is necessary to view the trend screen in order to activate some changes when in manual mode.
14. Once the cure cycle has been completed, vent the pressure, if any remains, and allow the temperature to drop.
15. Return to the door lock mechanism while standing completely to the right of the autoclave. Disengage the safety lever and turn on the hydraulics.
16. Unlock the door using the lever, then turn off the hydraulics.
17. Push the door open and leave it open if the part needs to continue cooling.
18. Prior to removing the part from the autoclave, detach the vacuum hose and turn off the vacuum pump.
19. Remove the part.
20. Log out of the software and shut down the computer. Again you may need to silence the alarm while the software closes.

21. Once the computer is off, switch the power lever to the “off” position.